Journal Pre-proofs

Improving aqueous solubility of paclitaxel with polysarcosine-*b*-poly(γ-benzyl glutamate) nanoparticles

Coralie Lebleu, Laetitia Plet, Florène Moussy, Gaëtan Gitton, Rudy Da Costa Moreira, Ludmilla Guduff, Barbara Burlot, Rodolphe Godiveau, Aïnhoa Merry, Sébastien Lecommandoux, Gauthier Errasti, Christiane Philippe, Thomas Delacroix, Raj Chakrabarti

PII: S0378-5173(22)01056-0
DOI: https://doi.org/10.1016/j.ijpharm.2022.122501
Reference: IJP 122501

To appear in: *International Journal of Pharmaceutics*

Received Date: 30 July 2022
Revised Date: 9 December 2022
Accepted Date: 12 December 2022

Please cite this article as: C. Lebleu, L. Plet, F. Moussy, G. Gitton, R. Da Costa Moreira, L. Guduff, B. Burlot, R. Godiveau, A. Merry, S. Lecommandoux, G. Errasti, C. Philippe, T. Delacroix, R. Chakrabarti, Improving aqueous solubility of paclitaxel with polysarcosine-*b*-poly(γ-benzyl glutamate) nanoparticles, *International Journal of Pharmaceutics* (2022), doi: https://doi.org/10.1016/j.ijpharm.2022.122501

Improving aqueous solubility of paclitaxel with polysarcosine-*b*-poly(γ-benzyl glutamate) nanoparticles

Coralie Lebleu,[1] Laetitia Plet,[1] Florène Moussy,[1] Gaëtan Gitton,[1] Rudy Da Costa Moreira,[1] Ludmilla Guduff,[1] Barbara Burlot,[1] Rodolphe Godiveau,[1] Aïnhoa Merry,[1] Sébastien Lecommandoux,[2] Gauthier Errasti,[1] Christiane Philippe,[1] Thomas Delacroix,[1] Raj Chakrabarti[1,3]*

[1] PMC Isochem SAS, 32, rue Lavoisier F-91710, Vert-Le-Petit, France

[2] Univ. Bordeaux, CNRS, Bordeaux INP, LCPO, UMR 5629, F-33600, Pessac, France

[3] Chakrabarti Advanced Technology, LLC, PMC Group Building, 1288 Route 73, Ste 110, Mount Laurel, NJ 08054, USA

*To whom correspondence should be addressed: raj@pmc-group.com

Orcid numbers:

Coralie Lebleu 0000-0003-1843-8599

Laetitia Plet 0000-0002-9413-6608

Sébastien Lecommandoux 0000-0003-0465-8603

Gauthier Errasti 0000-0001-7571-3257

Thomas Delacroix 0000-0001-8932-6899

Abstract

New stealth amphiphilic copolymers based on polysarcosine (PSar) rather than poly(ethylene glycol) (PEG) have gained more attention for their use as excipients in nanomedicine. In this study, several polysarcosine-*b*-poly(γ-benzyl glutamate) (PSar-*b*-PGluOBn) block copolymers were synthesized by ring opening polymerization (ROP) of the respective N-carboxyanhydrides (NCAs) and were characterized by Fourier-transform infrared spectroscopy (FTIR), proton nuclear magnetic resonance (^{1}H NMR) and size-exclusion chromatography (SEC). Copolymers had different PGluOBn block configuration (racemic L/D, pure L or pure D), degrees of polymerization of PSar between 28 and 76 and PGluOBn between 9 and 93, molar masses (M_n) between 5.0 and 24.6 kg.mol^{-1} and dispersities (Đ) lower than 1.4. Nanoparticles of PSar-*b*-PGluOBn loaded with paclitaxel (PTX), a hydrophobic anti-cancer drug, were obtained by nanoprecipitation. Their hydrodynamic diameter (D_h) ranged from 27 to 118 nm with polydispersity indexes (PDI) between 0.01 and 0.20, as determined by dynamic light scattering (DLS). Their morphology was more spherical for copolymers with a racemic L/D PGluOBn block configuration synthesized at 5 °C. PTX loading efficiency was between 63 and 92% and loading contents between 7 and 15%. Using PSar-*b*-PGluOBn copolymers as excipients, PTX apparent water-solubility was significantly improved by a factor up to 6600 to 660 µg.mL^{-1}.

Keywords: polysarcosine, poly(γ-benzyl glutamate), NCA polymerization, self-assembly, nanoparticles, paclitaxel

Graphical abstract

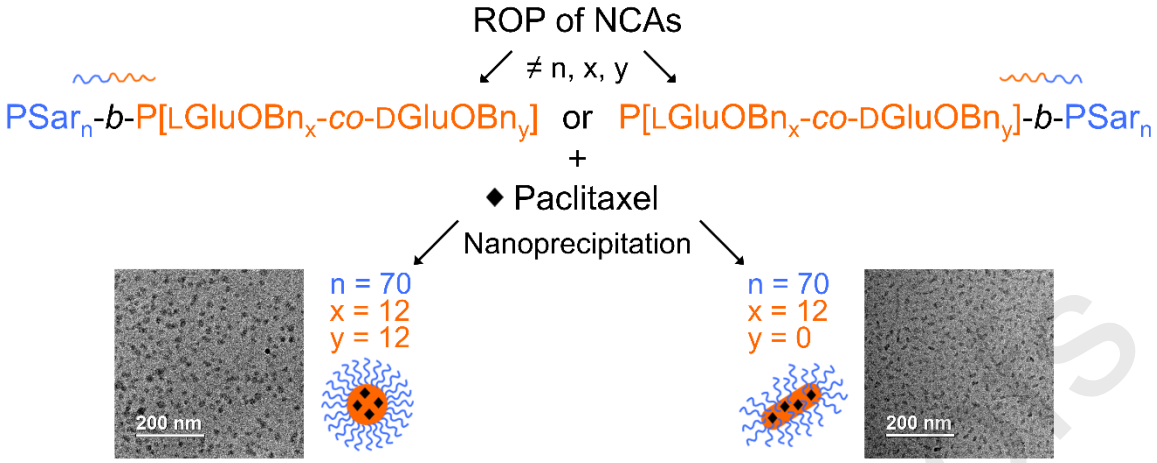

1 Introduction

Many active pharmaceutical ingredients (APIs) have a poor solubility in water, which limits their potential in clinics, especially for intraveneous (i.v.) administration. Drug discovery has led to an increasing number of new hydrophobic chemicals to the point where 90% of small molecules in discovery are considered poorly water-soluble,[1] which is one of the main reasons why many new drug candidates do not reach the market. Moreover, commercially available formulations of hydrophobic APIs are composed of excipients and/or co-solvents to improve their solubility, but may lead to poor safety and tolerability.[1] A good example is paclitaxel (PTX), one of the most widely used chemotherapeutic agents due to its potency against a variety of solid tumors including breast, ovarian, lung and head and neck cancers.[2] The first PTX formulation approved in 1998 by the Food and Drug Administration (FDA) for parenteral administration, Taxol®, was composed of PTX in a co-solvent system comprising polyoxyethylated castor oil (Cremophor® EL) and absolute ethanol at a 50/50 v/v ratio. Although it allowed the dissolution of PTX at 6 mg.mL^{-1}, this vehicle was responsible for severe side effects like hypersensitivity reactions.[3] To avoid the use of a co-solvent, new PTX formulations have been developed and are in various stages of clinical trials: an albumin-bound PTX Abraxane®, a liposome Lipusu®, and polymeric nanoparticles (NPs) Cynviloq IG-001/Genexol-PM and NK105.[4,5]

Such nano-sized drug delivery systems (DDSs) allow the solubilization of the hydrophobic API in water, but also have various advantages such as preventing premature drug degradation, enhancing drug uptake into tumors by passive targeting, controlling the drug's pharmacokinetic profile and thus improving its bioavailability.[6–9] As DDSs, polymeric nanoparticles made from amphiphilic block copolymers have attracted increasing interest.[10] Among them, polypept(o)ide-based NPs have the advantage of being biocompatible and biodegradable.[11–14] In the case of PTX, NK105 is an example among others of a polymeric formulation where PTX is loaded in poly(ethylene glycol)-*b*-polypept(o)ide (PEG-*b*-polypept(o)ide) micelles.[15–20] Even if poly(ethylene glycol) (PEG) is widely used as a hydrophilic block for its water-solubility and its stealthiness, it presents major drawbacks as it is not biodegradable and can trigger immunogenic responses.[21] Polysarcosine (PSar) has recently demonstrated its potential as a polypeptoide alternative to PEG since it has similar properties such as its hydrophilicity, stealthiness and low toxicity but has the advantage of being biodegradable as it is based on the endogenous amino acid derivative sarcosine, N-methyl glycine.[21–23] Notably, polypeptoide-*b*-polypeptide copolymers (copolypept(o)ides) based on PSar-*b*-polypeptide have been investigated as excipients to develop new DDSs.[11,23,24] Poly(γ-benzyl-L-glutamate) (PLGluOBn, pure L block) was found to be a suitable polypeptide hydrophobic block to load PTX,[20] and is a well-studied α-helical rod-like polymer to form DDSs.[25–29] PSar-*b*-PLGluOBn copolypept(o)ides with a PSar block from 182 up to 400 repeat units have been investigated by Barz and coworkers in different fields of application,[30,31] including cancer.[11,32] PSar-*b*-P(LGluOBn-*co*-DGluOBn) copolypept(o)ides with a racemic PGluOBn block and a PSar block with more than 125 repeat units were used as excipients to solubilize hydrophobic APIs including PTX.[24] For this study, we designed various polysarcosine-*b*-poly(γ-benzyl glutamate) (PSar-*b*-PGluOBn) copolypept(o)ides of varying molar mass, hydrophilic fraction and PGluOBn block configuration (racemic, pure L or pure D), to investigate the impact on the self-assembly and PTX loading. The technical and cost constraints of industrial scale-up were also considered. For this purpose, copolymers with shorter molar masses than those of the prior art[23,24,11] were designed to facilitate synthesis and yield less expensive products in the perspective of commercial applications. Here, we report the synthesis and characterization of different PSar-*b*-PGluOBn copolymers as well as the formulation and characterization of PTX-loaded nanoparticles resulting from their self-assembly.

2 Materials and methods

2.1 Materials

Neopentylamine was purchased from TCI Europe. Paclitaxel was purchased from Key Organics. LGluOBn NCA, DGluOBn NCA and Sar NCA were sampled from PMC Isochem batches. DMF NORMAPUR® grade with a maximum water content of 0.05%, was purchased from Avantor. Ethyl acetate and methyl *tertiary*-butyl ether (MTBE) were purchased respectively from Brenntag and Univar. Acetonitrile (HPLC grade) was purchased from VWR. α-Cyano-4-hydroxycinnamic acid (α-CHCA, used as the matrix for MALDI-TOF experiments, was of the highest grade available and used without further purification) was purchased from Sigma Aldrich. Water was ultrapure grade. Unless stated otherwise, materials and solvents were used as such and the temperature was room temperature (22 – 28 °C).

2.2 Instrumentation

2.2.1 FTIR

NCA polymerization was monitored by Fourrier-transform infrared (FTIR) spectroscopy on a Thermo Scientific Nicolet iS5 spectrometer equipped with an ID7 ATR module. Data were processed using OMNIC 9.7 software. Polymerizations were stopped when NCA-associated carbonyl bands at 1850 and 1778 cm^{-1} had disappeared, corresponding to the total NCA consumption. Purified polymers were also analyzed by FTIR in solid state.

2.2.2 ^{1}H NMR

2.2.2.1 ^{1}H NMR at 80 MHz

Proton Nuclear Magnetic Resonance (^{1}H NMR) spectroscopy was performed on a 80 MHz MAGRITEK Spinsolve 80 Carbon, with the following parameters: NS = 64, repetition time = 10 to 30 s, pulse angle = 90, by dissolving the product in deuterated water (D_2O) or dimethylsulfoxide (DMSO-d_6) at a concentration between 20 and 50 $g.L^{-1}$. Data were processed using SpinSolve and MestReNova softwares. ^{1}H NMR was used to determine degrees of polymerization (n) of the PSar block and composition (x+y) of the PGluOBn block. Calibration was performed on the signal at 0.84 ppm of the 9 protons of the *t*-butyl chain-end of the neopentylamine initiator. Signal of the methyl protons of PSar segment at 3.10 – 2.67 ppm was used to evaluate n, and signals of the benzyl and the methylene protons of PGluOBn block respectively at 7.28 and 5.01 ppm were used to assess (x+y).

2.2.2.2 ^{1}H-DOSY NMR at 600 MHz

Diffusion-ordered spectroscopy was subcontracted to GreenPharma and performed on a Brüker Avance DRX-600 MHz spectrometer equipped with a cryoprobe-head. The product (10 mg) was dissolved in DMSO-d_6 (600 µL). Spectra were acquired with the *ledbpgp2s* pulse program from Bruker Topspin software with the following parameters for $PSar_{66}$-*b*-$PLGluOBn_{23}$: ns=8, p30=1.9ms, p19=1.0ms, d20=180ms, d21=5ms, d16=200us, 1_TD=32, GAB d1=10s, G=6.44 Gauss/mm. The same parameters were used for PSar **S1** except the following ones that were adapted: p30=1.5ms, d20=100ms. Data were processed using MestReNova software with the peak fit algorithm, 65536 points in the F2 dimension, 128 points in the F1 dimension and an auto decay component (multi-exponential processing).

2.2.3 MALDI-TOF MS

Matrix Assisted Laser Desorption Ionization/Time Of Flight (MALDI-TOF/TOF) UltrafleXtreme mass spectrometry (MS) was performed on a Bruker Daltonics mass spectrometer. Mass spectra were obtained in linear or reflector positive ion mode. The laser intensity was set just above the ion generation threshold to obtain peaks with the highest possible signal-to-noise (S/N) ratio without significant peak broadening. All data were processed using the FlexAnalysis software package (Bruker Daltonics). Polysarcosine samples were solubilized in methanol at 10 g/L and diluted to 0.5 g/L in the matrix composed of α-cyano-4-hydroxycinnamic acid (CHCA) at 10 g/L in an acetonitrile/water 1/1 v/v mixture. Three deposits of 1 µL of the diluted solution were made on the MALDI plate. A close external calibration was carried out using PEG (1000, 2000 and 3500 g/mol).

2.2.4 SEC in DMF

2.2.4.1 SEC in DMF with RI detector

Size-exclusion chromatography (SEC) analyses in DMF in the presence of 0.45%w/v LiBr were performed on an Agilent 1260 LC equipped with a diode array detector (DAD) and a differential refractive index detector (dRI) and a three-column set of PSS GRAM analytical columns (100 Å, 8 x 300 mm, 10 µm; 100 Å, 8 x 300 mm, 10 µm; 1000 Å, 8 x 300 mm, 10 µm) with exclusion limits from 100 to 1 000

000 g.mol^{-1}. Analyses were carried out on samples prepared in DMF + LiBr at 45 °C using the same solvent as eluent at a flow rate of 1 mL.min^{-1} and filtered on a 0.45 µm hydrophilic polytetrafluoroethylene (H-PTFE) syringe filter. Data were acquired and processed with OpenLAB Chemstation software.

SEC for the characterization of copolymers

To determine the number average molar mass (M_n) and dispersity (Đ) of polymers and copolymers, analyses were carried out on polymer samples prepared at 4 g.L^{-1}. EasiVial kit of polystyrenes (PS) from Agilent was used as standard (266 to 66 000 g.mol^{-1}). And data were further processed with Cirrus add-on.

SEC for the characterization of nanoparticles

To determine the copolymer concentration in the PTX-loaded nanoparticles ($[C]_{NPs}$), a volume of 400 µL of each sample of NPs was dried using a centrifugal evaporator (SP Genevac EZ2, water evaporation automatic program). The samples injected in SEC were prepared by dissolving the dried sample in 1 mL of DMF + LiBr, hence a dilution by 2.5).

A standard curve in DMF + LiBr was prepared for each copolymer with concentrations ([C]) between 1 and 4 g.L^{-1}. Linear regression of the area obtained for the RI signal versus [C] was plotted for each copolymer to obtain standard curve equations.

For each formulated sample, $[C]_{NPs}$ was determined using the peak area obtained and the appropriate standard curve equation, and then multiplying by the factor of dilution.

Copolymer recovery (CR) was calculated as the ratio of $m(C)_{NPs}$ (obtained using $[C]_{NPs}$) divided by the mass of copolymer initially fed in the NPs' preparation.

Drug loading content (DLC) of the PTX-loaded NPs was calculated as the ratio of the mass of PTX recovered at the final stage of the NPs' preparation ($m(PTX)_{NPs}$, obtained by UPLC) divided by the mass of the NPs; the mass of NPs being the sum of the mass of copolymer (obtained using $[C]_{NPs}$ by SEC) and $m(PTX)_{NPs}$.

2.2.4.2 SEC in DMF with RI and LS detectors

Another SEC chain in DMF equipped with a light scattering detector was also used to analyze the copolymers. SEC analyses in DMF in the presence of 1 g.L^{-1} LiBr were performed on ThermoScientific UltiMate 3000 chromatography system equipped with a DAD, DRI detector and a multi-angle light scattering detector (MALS) from Wyatt technology, and two Shodex Asahipak GF310 and GF510 columns (7.5 x 300 mm, 5 µm) with exclusion limits from 500 to 300 000 g.mol^{-1}. Polymer samples were solubilized at 5 g.L^{-1} in DMF + LiBr for 24h and filtered on a 0.45 µm PTFE syringe filter. Analyses were carried out at 50 °C using the same solvent as eluent at a flow rate of 0.5 mL.min^{-1}. Toluene was used as a flow marker. Data were acquired and processed with Astra software. The absolute number average molar mass (M_n) and dispersity (Đ) of copolymers was determined using a calibration of columns made with PS standards. The molar mass distribution was obtained by LS using dn/dc of PS = 0.1590 mL.g^{-1}).

2.2.5 SEC in H_2O/ACN

SEC analyses in water/acetonitrile/trifluoroacetic acid (H_2O/ACN/TFA) 60/40/0.1 v/v/v were performed on a Malvern Panalytical Omnisec Resolve and Reveal equipped with a UV detector, dRI detector, RALS-LALS detector and a set of 3 Waters Ultrahydrogel columns (two columns 250 Å, 7.8 x 300 mm, 6 µm and one column 500 Å, 7.8 x 300 mm, 10 µm) with exclusion limits from 1 000 to 400 000 g.mol^{-1}. Analyses were carried out on polymer samples prepared in H_2O/ACN/TFA 60/40/0.1 v/v/v at 38 °C using the same solvent as eluent at a flow rate of 0.7 mL.min^{-1} and filtered on a 0.2 µm nylon syringe filter. Data were acquired and processed with Omnisec software. The dn/dc of polysarcosine **S1** (purity 98.4%) was determined at 0.1545 mL.g^{-1} with this system by performing a calibration using seven different concentrations. This dn/dc was used to determine the true number average molar mass (M_n) and dispersity (Đ) of PSar **S1** and **S2**.

2.2.6 CMC determination

Critical micellar concentration (CMC) determination was subcontracted to DataPhysics Instruments. Surface tension was measured with a Dynamic contact angle tensiometer DCAT 25 at room temperature using the Wilhelmy plate method (19.9 mm length and 0.2 mm thickness) on a series of dilutions of a polymer suspension in water starting at 0.5 mmol/L (stirring duration of 2 minutes per dilution step).

2.2.7 DLS

Dynamic light scattering (DLS) measurements were carried out on a Zetasizer Pro (Malvern Panalytical) equipped with a He-Ne laser (633 nm), at 25 °C and a scattering angle of 174.8°. Software used was ZS Explorer. A low volume plastic cell of 10 mm optical path length was filled with 70 µL of sample. Viscosity of the dispersant was corrected according to the solvent or mixture of solvents used. Data were acquired on three different measurements with an automatic optimization of the number and duration of runs per measurement. Results are expressed as an average of these measurements. D_h of the objects is the intensity mean for each population. PDI is calculated from the autocorrelation functions using the cumulant method. Procedure for the determination of PSar molar mass by DLS was adapted from literature.[22] Briefly, solutions of **S1** and **S2** were prepared at 10 g/L in PBS by overnight dissolution followed by filtration on a 0.2 µm polyethersulfone (PES) syringe filter. Weight average molar mass (M_w) was determined using the measured hydrodynamic radius (R_h) and the relation from literature: $R_h = 0.041 {M_w}^{0.45}$.

2.2.8 Zeta-potential

Zeta-potential (ZP) measurements were carried out on a Zetasizer Pro (Malvern Panalytical) equipped with a He-Ne laser (633 nm), at 25 °C and a scattering angle of 174.8°. Software used was ZS Explorer. A folded capillary cell (DTS1070) was filled with 1 mL of sample diluted 1:100 in water. Data were acquired over six different automatic measurements. Zeta-potential (ZP) values and ZP deviations are expressed as an average and standard deviation of these six measurements.

2.2.9 UPLC

Ultra-performance liquid chromatography (UPLC) measurements were performed on an Acquity UPLC H-class from Waters equipped with a reversed-phase column (Acquity BEH, C18, 130 Å, 50 mm x 2.1 mm x 1.7 µm, Waters) and a diode array detector (DAD) Acquity eλ from Waters. Data were acquired and processed with Empower 3 software. The gradient elution was performed with 2 solvents: solvent A was water in the presence of 0.05 %v/v trifluoroacetic acid (TFA) and solvent B acetonitrile in the presence of 0.05 %v/v TFA. Column was equilibrated for at least 30 min at a A:B mixture of 80:20. The sequence duration was 8 min with the following gradient of A:B solvents: 0 – 2.5 min 80:20, 2.5 – 4 min 5:95, 4 – 8 min 80:20. Eluents were degassed by the machine. Flow rate was 0.6 mL.min^{-1}. Column temperature was 35 °C. Injected volume was 3 µL. UV detector was set at 254 nm. Typical retention time of PTX was 2.24 min.

Loading efficiency (LE) of the PTX-loaded NPs was determined by UPLC. The injected samples were prepared by dissolving 90 µL of NPs in 910 µL of ACN:DMF 90/10 v/v (hence a dilution by 11.1) followed by a filtration with a 0.2 µm H-PTFE syringe filter.

A standard curve in ACN:H_2O:DMF 90:9:1 v/v/v was prepared with PTX concentrations ([PTX]) between 50 and 200 µg.mL^{-1}. Linear regression of the area at 254 nm versus [PTX] was plotted to obtain the standard curve equation.

For each formulated sample, PTX concentration in nanoparticles ($[PTX]_{NPs}$) was determined using the peak area obtained and the standard curve equation, and then multiplying by the factor of dilution.

LE was calculated as the ratio of $m(PTX)_{NPs}$ (obtained using $[PTX]_{NPs}$) divided by the mass of PTX initially fed in the NPs' preparation.

2.2.10 HS-GC

Headspace gas chromatography (HS-GC) was used to dose the content of DMF as a residual solvent in formulations. HS-GC were performed on an Agilent 7890B GC system equipped with split/splitless injector, a flame ionization detector (FID), an Agilent 7697A autosampler and using a CP Sil 5CB column (50 m length, 0.32 mm diameter, 5 µm film thickness). A known quantity of sample was introduced into a 20 mL crimp vial and dissolved with a few milliliters of a low volatile solvent (water, DMSO or NMP).

The vial was crimped and incubated in order to reach an equilibrium of concentration of the residual solvent between the liquid phase and the gas phase. The headspace of the vial was then injected into the GC system via a split injector and the residual solvent was detected by FID. Data were acquired and processed using OpenLAB Chemstation software.

2.2.11 Cryo-TEM

Cryo-transmission electron microscopy (cryo-TEM) images were recorded on a LaB6 JEOL 2100 (JEOL, Japan) operating at 200 kV. The samples were prepared by placing a drop of a nanoparticle suspension on a holey carbon grid (Quantifoil Micro Tools GmbH, Germany). Excess solution was blotted off with a filter paper. The grid was quickly immersed in liquid ethane, placed on a Gatan 626 cryo-holder and transferred to the microscope. The grids were observed at low temperature (-180 °C) and under low dose conditions (JEOL minimum dose system). Pictures were taken with an Ultrascan 1000 with a 2k x 2k CCD camera (Gatan, USA) and analyzed with ImageJ software.

2.3 Methods

2.3.1 $PSar_n$ synthesis

Typically, Sar NCA (35.0 g, 304 mmol, 28 eq) was dissolved in dry DMF (350 mL) at room temperature followed by the addition of neopentylamine as initiator (1276 µL, 10.8 mmol, 1 eq). The reaction mixture was stirred at room temperature and after the end of CO_2 evolution, completion of the reaction was confirmed by FTIR spectroscopy (disappearance of the NCA carbonyl peaks at 1853 and 1786 cm^{-1}). Precipitation of the polymer was performed at room temperature by pouring the reaction mixture over 1.4 L of ethyl acetate under vigorous stirring. After filtration, the product was reslurried and washed twice with 125 mL of ethyl acetate and then dried under vacuum. $PSar_{28}$ (**S2**) was obtained with a yield of 85%.

^{1}H NMR: $PSar_{28}$ (**S2**) (80 MHz, D_2O): δ [ppm] = 4.63 – 4.04 (55H (2n), br, CO-C**H$_2$**-NCH_3-), 3.30 – 2.78 (90H (3n), br, -NC**H$_3$**-), 0.90 (9H, d, C(C**H$_3$**)-CH_2-NH, initiator moiety).

2.3.2 $PSar_n$-*b*-P(LGluOBn$_x$-*co*-DGluOBn$_y$) synthesis using $PSar_n$ block as macroinitiator

PSar block **S1** (M_n = 5.3 kg.mol^{-1}, 0.7 g, 0.13 mmol, 1.0 eq) was dissolved in dry DMF (17 mL) at room temperature. A mixture of LGluOBn NCA (1.7 g, 6.38 mmol, 49 eq) and DGluOBn NCA (1.7 g, 6.38 mmol, 49 eq) powders was added to the reaction medium. The reaction mixture was stirred at 5 °C and after the end of CO_2 evolution, completion of the reaction was confirmed by FTIR spectroscopy. Precipitation of the copolymer was performed at room temperature by pouring the reaction mixture over 170 mL of MTBE under vigorous stirring. After filtration, the product was reslurried and washed with 2 x 30 mL of MTBE and then dried under vacuum. Copolymer $PSar_{58}$-*b*-P(LGluOBn$_{40}$-*co*-DGluOBn$_{40}$) (**4b**) was obtained with a yield of 76%.

^{1}H NMR: $PSar_{58}$-*b*-P(LGluOBn$_{40}$-*co*-DGluOBn$_{40}$) (**4b**) (80 MHz, DMSO-d_6): δ [ppm] = 8.12 (69H (x+y), br,-N**H**-, labile H), 7.27 (394H (5(x+y)), s, -C_6**H$_5$**), 5.01 (160H (2(x+y)), s, -C**H$_2$**-C_6H_5), 4.67 – 3.67 (189H (2n+1(x+y)), br, CO-C**H$_2$**-NCH_3- and CO-C**H**-NH), 3.13 – 2.65 (174H (3n), br, -NC**H$_3$**-), 2.41 – 1.37 (270H (4(x+y), br, -CH-C**H$_2$**-C**H$_2$**-CO), 0.83 (9H, d, C(C**H$_3$**)-CH_2-NH, initiator moiety).

2.3.3 $PSar_n$-*b*-P(LGluOBn$_x$-*co*-DGluOBn$_y$) synthesis using the one-pot polymerization method

Sar NCA (3.4 g, 29.6 mmol, 70 eq) was dissolved in dry DMF at room temperature followed by the addition of neopentylamine as initiator (49.9 µL, 0.42 mmol, 1 eq). The reaction was stirred at room temperature and after the end of CO_2 evolution, completion of the reaction was confirmed by FTIR spectroscopy. To the reaction medium containing PSar was added LGluOBn NCA (1.2 g, 4.52 mmol, 11 eq) and DGluOBn NCA (1.2 g, 4.52 mmol, 11 eq) previously weighted and mixed. After 20 h at room temperature, total consumption of NCAs was confirmed by FTIR spectroscopy. Precipitation of the copolymer was performed at room temperature by pouring the reaction mixture over 300 mL of MTBE under vigorous stirring. After filtration, the product was reslurried with 2 x 100 mL of MTBE and then dried under vacuum. Copolymer $PSar_{76}$-*b*-P(LGluOBn$_9$-*co*-DGluOBn$_9$) (**3b**) was obtained with a yield of 54%.

^{1}H NMR: $PSar_{76}$-*b*-P(LGluOBn$_9$-*co*-DGluOBn$_9$) (**3b**) (80 MHz, DMSO-d_6): δ [ppm] = 8.41 – 7.86 (17H (x+y), br,-N**H**-, labile H), 7.29 (84H (5(x+y)), s, -C_6**H$_5$**), 5.03 (38H (2(x+y)), s, -C**H$_2$**-C_6H_5), 4.75 – 3.73

(147H (2n+1(x+y)), br, CO-C**H**$_2$-NCH$_3$- and CO-C**H**-NH), 3.17 – 2.62 (227H (3n), br, -NC**H**$_3$-), 2.40 – 1.41 (63H (4(x+y)), br, -CH-C**H**$_2$-C**H**$_2$-CO), 0.84 (9H, s, C(C**H**$_3$)-CH$_2$-NH, initiator moiety).

2.3.4 P(LGluOBn$_x$-*co*-DGluOBn$_y$)-*b*-PSar$_n$ synthesis

LGluOBn NCA (1.6 g, 6.0 mmol, 12 eq) and DGluOBn NCA (1.6 g, 6.0 mmol, 12 eq) were dissolved in 40 mL of dry DMF at room temperature followed by the addition of neopentylamine as initiator (58.5 µL, 0.50 mmol, 1 eq). The reaction mixture was stirred at room temperature and after the end of CO_2 evolution, completion of the reaction was confirmed by FTIR spectroscopy. Sar NCA (4.0 g, 34.8 mmol, 70 eq) was then added to the reaction mixture. Again, the reaction mixture was stirred at room temperature and after the end of CO_2 evolution, completion of the reaction was confirmed by FTIR spectroscopy. Precipitation of the copolymer was performed at room temperature by pouring the reaction mixture over 300 mL of MTBE under vigorous stirring. After filtration, the product was reslurried with 200 mL and then 100 mL of MTBE and then dried under vacuum. Copolymer P(LGluOBn$_{13}$-*co*-DGluOBn$_{13}$)-*b*-PSar$_{75}$ (**9**) was obtained with a yield of 89%.

^{1}H NMR: P(LGluOBn$_{13}$-*co*-DGluOBn$_{13}$)-*b*-PSar$_{75}$ (**9**) (80 MHz, DMSO-d_6): δ [ppm] = 8.57 – 7.85 (23H (x+y), br,-N**H**-, labile H), 7.28 (116H (5(x+y)), s, -C$_6$**H**$_5$), 5.02 (52H (2(x+y)), s, -C**H**$_2$-C$_6$H$_5$), 4.73-3.77 (158H (2n+1(x+y)), br, CO-C**H**$_2$-NCH$_3$- and CO-C**H**-NH), 3.16-2.63 (224H (3n), br, -NC**H**$_3$-), 2.41-1.39 (91H (4(x+y), br, -CH-C**H**$_2$-C**H**$_2$-CO), 0.77 (9H, s, C(C**H**$_3$)-CH$_2$-NH, initiator moiety).

2.3.5 P(LGluOBn$_x$-*co*-DGluOBn$_y$)-*b*-PSar$_n$-Ac synthesis

P(LGluOBn$_{13}$-*co*-DGluOBn$_{13}$)-*b*-PSar$_{75}$ (9) (**M_n** = 7.0 kg.mol^{-1}, 1.0 g, 0.143 mmol, 1 eq) was dissolved in 10 mL of dry DMF at room temperature followed by the addition of DMAP (17.5 mg, 0.14 mmol, 1 eq), and NMM (172.8 µL, 1.57 mmol, 11 eq). After full dissolution, acetic anhydride (135.0 µL, 1.43 mmol, 10 eq) was added and the reaction mixture was stirred overnight at room temperature. Precipitation of the resulting copolymer was performed at room temperature by pouring the reaction mixture over 50 mL of MTBE under vigorous stirring. After filtration, the product was reslurried with 2 x 10 mL of MTBE and then dried under vacuum. Copolymer P(LGluOBn$_{11}$-*co*-DGluOBn$_{11}$)-*b*-PSar$_{68}$-Ac (10) was obtained with a yield of 77%.

^{1}H NMR: P(LGluOBn$_{11}$-*co*-DGluOBn$_{11}$)-*b*-PSar$_{68}$-Ac (**10**) (80 MHz, DMSO-d_6): δ [ppm] = 8.51-7.78 (21H (x+y), br,-N**H**-, labile H), 7.28 (103H (5(x+y)), s, -C$_6$**H**$_5$), 5.01 (47H (2(x+y)), s, -C**H**$_2$-C$_6$H$_5$), 4.68-3.57 (154H (2n+1(x+y)), br, CO-C**H**$_2$-NCH$_3$- and CO-C**H**-NH), 3.16-2.59 (205H (3n), br, -NC**H**$_3$-), 2.32-1.44 (73H (4(x+y), br, -CH-C**H**$_2$-C**H**$_2$-CO), 0.84 (9H, d, C(C**H**$_3$)-CH$_2$-NH, initiator moiety).

2.3.6 Preparation of PTX-loaded nanoparticles

Each PSar-*b*-PGluOBn copolymer described in this work (**1–10**) was tested separately with the following formulation procedure, adapted from the literature.[11] Solutions of one type of copolymer and PTX were prepared in DMF at 200 g.L^{-1} and 20 g.L^{-1}, respectively. A solution of PTX was prepared in DMF at 20 g.L^{-1}. A solution at a feed weight ratio (FWR) of 10% was prepared in DMF at a copolymer concentration of 100 g.L^{-1} and a PTX concentration of 10 g.L^{-1}. Using a syringe pump (Fusion 100-X, Chemyx), 1 mL of this organic solution was injected at a flow rate (FR) of 30 mL.min^{-1} in 9 mL of ultrapure water under 400 rpm stirring. After complete addition, stirring was pursued for 5 min. The nanoparticle suspensions freshly obtained in a H_2O/DMF mixture at 9/1 v/v were purified to remove DMF and unloaded drug by a first filtration on a 0.2 µm PES syringe filter, followed by a gel filtration column (PD-10 desalting, Cytiva, gravity flow) using phosphate buffer saline (PBS, 1X) as eluent to recover purified nanoparticles in PBS. Fractions containing PTX were combined, volume was measured to determine the column dilution factor (DF). Finally, a second filtration on a 0.2 µm PES syringe filter was performed to mimic sterile filtration.

This procedure was adapted for the screening of the procedure conditions using PSar$_{58}$-*b*-P(LGluOBn$_{40}$-*co*-DGluOBn$_{40}$) (**4b**): FWR of 5, 10 and 20% and FR of 1, 10 and 30 mL.min^{-1} were tested. To adapt FWR, the copolymer concentration in DMF was maintained at 100 g.L^{-1}, and the PTX concentration in DMF was varied at 5, 10 or 20 g.L^{-1}. For FWR 20%, copolymer and PTX were weighted in the same flask to directly obtain a solution at 100 g.L^{-1} of copolymer and 20 g.L^{-1} of PTX (since PTX was not soluble at 40 g.L^{-1} at room temperature).

3 Results and discussion

3.1 PAA synthesis and characterization

Polysarcosine$_n$-*b*-poly((γ-benzyl L-glutamate)$_x$-*co*-(γ-benzyl D-glutamate)$_y$) (PSar$_n$-*b*-P(LGluOBn$_x$-*co*-DGluOBn$_y$)) block copolymers were synthesized by ring opening polymerization (ROP) of corresponding α-amino acid N-carboxyanhydrides (NCAs) in N,N-dimethylformamide (DMF). Two PSar blocks with different molar masses were prepared (**Scheme 1**, *STEP A*): the polymer **S1**, a PSar$_{70}$ of 5 kg.mol^{-1} and **S2**, a PSar$_{28}$ of 2 kg.mol^{-1}. These PSar molar masses were chosen since they are lower than those of the prior art,[23,24,11] and also because they are often used for PEG,[33–35] and equivalence between molar mass of PEG and PSar has already been shown in the literature.[22] The ring opening polymerization of Sar NCA was initiated by neopentylamine and its consumption was followed by Fourier-transform infrared (FTIR) spectroscopy with the disappearance of carbonyl peaks at 1853 and 1786 cm^{-1}. These two PSar were synthesized on a scale of several tens of grams in order to polymerize the GluOBn block starting with the same macroinitiator batch to have no variability of PSar length in the final copolymers. After isolation and purification, both PSar were characterized by ^{1}H NMR spectroscopy, SEC, MALDI-TOF MS and DLS. **S1** and **S2** were obtained with a yield from 70 to 85% and a dispersity lower than 1.22. The results obtained were in good agreement with the theoretical values (**Table S1, Figures S1, S2**).

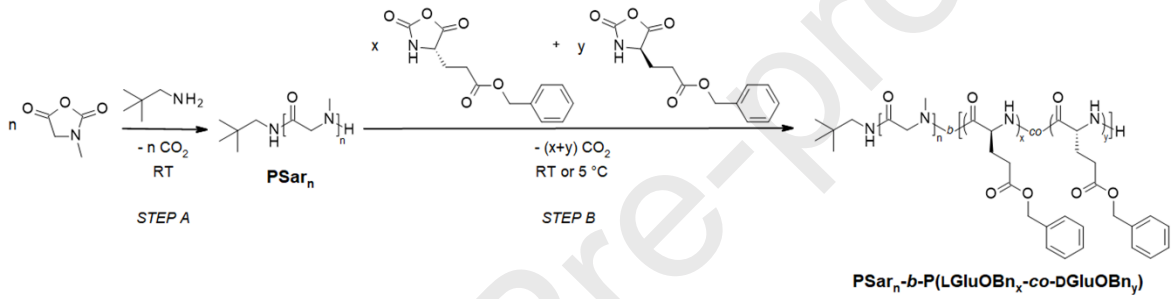

Scheme 1. Two-steps synthesis of PSar$_n$-*b*-P(LGluOBn$_x$-*co*-DGluOBn$_y$) copolymers: STEP A, ROP of Sar NCA using neopentylamine as initiator; and STEP B, ROP of LGluOBn and/or DGluOBn NCAs using PSar synthesized in STEP A as macroinitiator.

Then, the PSar block (**S1** or **S2**) was used as macroinitiator for the synthesis of the hydrophobic PGluOBn block. Lengths of the PGluOBn block were chosen to reach two different hydrophilic weight fractions (*f*): 50% and 20%. *f* was defined as the ratio of the M_n of the PSar block to the M_n of the whole copolymer and the M_n used in this calculation are the ones determined by ^{1}H NMR. In the first set of experiments, GluOBn NCA was introduced as a racemic mixture of LGluOBn NCA and DGluOBn NCA in order to obtain a racemic hydrophobic block (**Scheme 1**, *STEP B*). Degrees of polymerization (n) of the PSar block and composition (x+y) of the PGluOBn block were determined by ^{1}H NMR. Calibration was performed on the signal at 0.84 ppm of the 9 protons *t*-butyl chain-end of the neopentylamine initiator. Signal of the methyl protons of PSar segment at 3.10 – 2.67 ppm was used to evaluate n, and signals of respectively the benzyl and the methylene protons of PGluOBn block at 7.28 and 5.01 ppm were used to assess (x+y) (**Figure 1, S3–S9**). The characteristics of the obtained copolymers are summarized in **Table 1**.

As expected, degrees of polymerization of the PSar block in the four copolymers were close to the values determined with the ^{1}H NMR spectrum of respective PSar macroinitiators **S1** and **S2**. Likewise, the polymerization degrees of PGluOBn blocks (x+y) were very close to the expected values for all four copolymers leading to hydrophilic fractions *f* of 50% and 48% for respectively PSar$_{28}$-*b*-P(LGluOBn$_{4.5}$-*co*-DGluOBn$_{4.5}$) (**1**) and PSar$_{70}$-*b*-P(LGluOBn$_{13}$-*co*-DGluOBn$_{13}$) (**3a**), and 21% for PSar$_{28}$-*b*-P(LGluOBn$_{17}$-*co*-DGluOBn$_{17}$) (**2**) and PSar$_{75}$-*b*-P(LGluOBn$_{46}$-*co*-DGluOBn$_{46}$) (**4a**). SEC analyses showed well-defined copolymers with dispersities lower than 1.24 (slightly higher dispersity of 1.45 in the case of PSar$_{28}$-*b*-P(LGluOBn$_{17}$-*co*-DGluOBn$_{17}$) (**2**)) (**Figure 2, S10**) and apparent molar masses in good agreement with theoretical values. Finally, all copolymers were obtained in rather high yields between 70 and 76%.

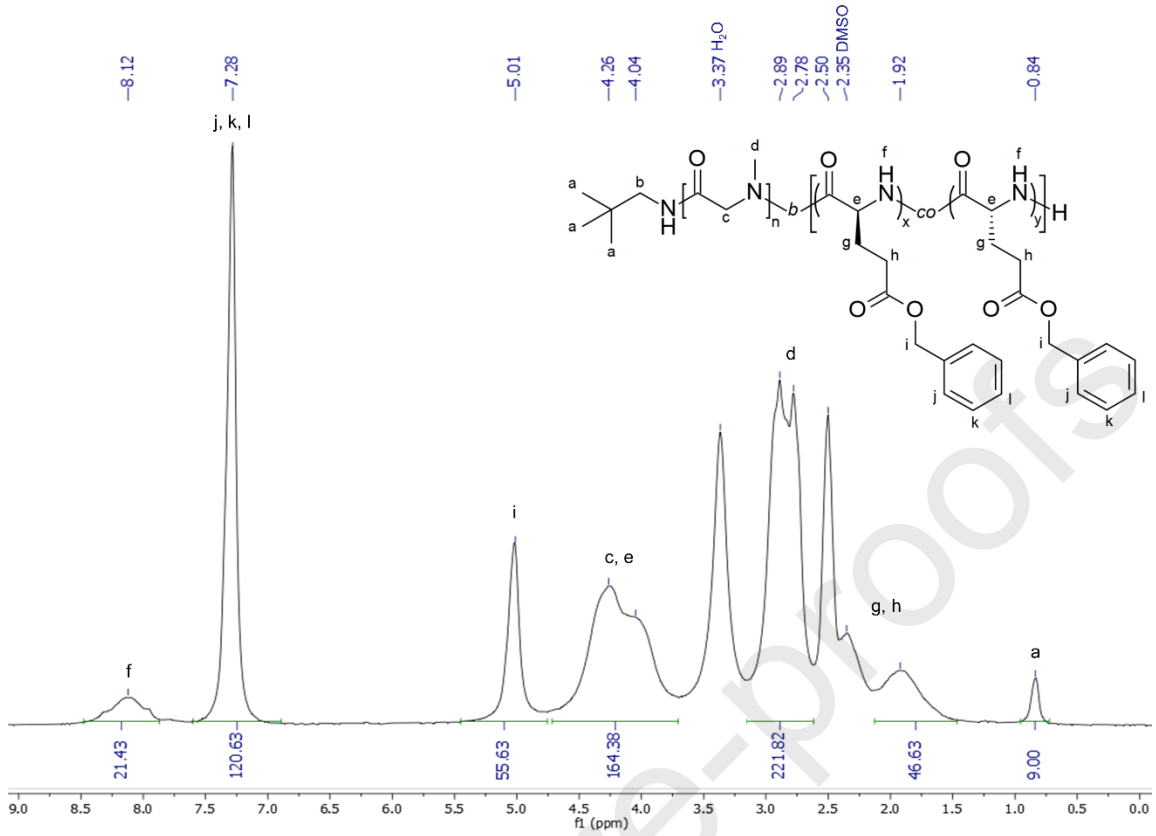

Figure 1. ^{1}H NMR spectrum (80 MHz) of the PSar$_{70}$-*b*-P(LGluOBn$_{13}$-*co*-DGluOBn$_{13}$) (**3a**) copolymer in DMSO-d_6 and its chemical structure.

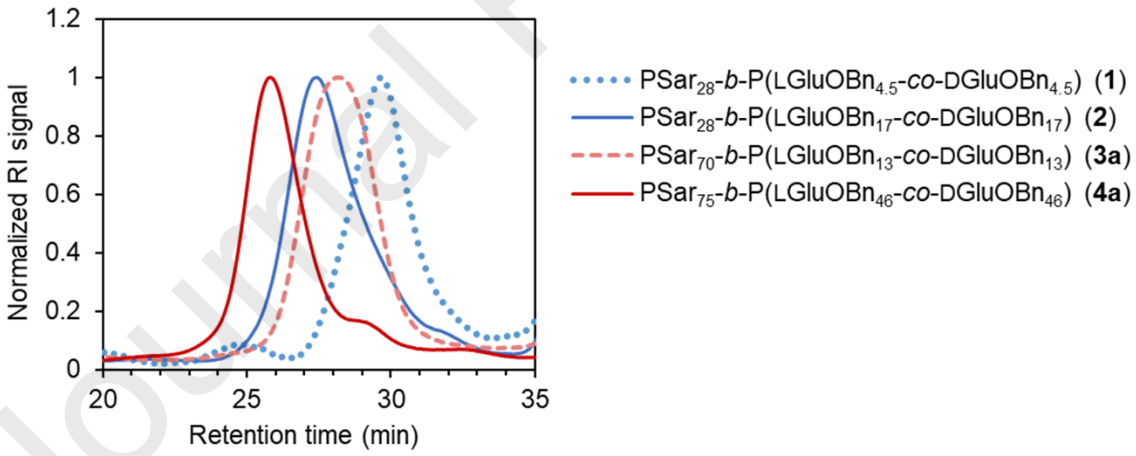

Figure 2. SEC traces (DMF, RI detection) of four PSar$_n$-*b*-P(LGluOBn$_x$-*co*-DGluOBn$_y$) copolymers.

The possibility of using a one-pot polymerization method was also explored. For this purpose, after total consumption of the Sar NCA monitored with FTIR spectroscopy, the LGluOBn and DGluOBn NCAs were added as a mix of powders, without any intermediate isolation and purification of the PSar block. The engaged mass of NCAs was always calculated to achieve the targeted hydrophilic weight fraction *f*. The copolymer (PSar$_{76}$-*b*-P(LGluOBn$_9$-*co*-DGluOBn$_9$) (**3b**), **Table 1***)* was obtained with a lower yield (54%) and presented a lower molar mass than the theoretical value of 10 kg.mol^{-1}: 9.3 kg.mol^{-1} (^{1}H NMR, **Figure S5**) and 7.9 kg.mol^{-1} (SEC, **Figure S10**). Furthermore, the hydrophilic fraction of 58% is significantly higher than the 50% aimed value. These observations are slightly different from the results reported by Birke *et al.*[11] who evidenced similar results whether a sequential approach or a one-pot synthesis was used. As they mentioned, both have advantages: in the sequential approach, the intermediate characterization of the block that will be used as macroinitiator allows for better adjustment

of the number of equivalents for the second block polymerization, while the one-pot method is faster and more practical from a process scale-up perspective. We chose the sequential method with the objective to get better control over the PSar length and hydrophilic fraction of the resulting copolymer and more comparable results by using the same PSar macroinitiator batch.

In a first attempt to synthesize the targeted copolymer $PSar_{70}$-*b*-P(LGluOBn$_{45}$-*co*-DGluOBn$_{45}$), the PGluOBn block was polymerized at room temperature (batch $PSar_{76}$-*b*-P(LGluOBn$_{47}$-*co*-DGluOBn$_{47}$) (**4c**)) and led to a total consumption of GluOBn NCA (controlled by FTIR spectroscopy), which is consistent with the n and (x+y) values found by ^{1}H NMR (**Figure S9**). Nevertheless, the SEC analysis highlights a lack of control of the polymerization in this case, leading to a smaller than expected M_n and higher dispersity (**Table 1**, **Figure S10**). The phenomenon of chain-end cyclization may be observed in this case, especially as the length of the PGluOBn block is high (90 repeat units) and therefore the polymerization time is longer. This intramolecular reaction of amidation between the primary amine end-group and the benzyl ester lateral group of the last GluOBn repeat unit leads to the termination of the macromolecular growing chain. Indeed, Heise and coll.[36] showed by mass spectrometry analyses that chains with pyroglutamate end-groups are no longer present when polymerization is conducted at 0 °C. Other studies supported this result and demonstrated that polymerizing the PGluOBn block at a low temperature (between 0 °C and 5 °C) reduces the occurrence of this undesired termination reaction.[37–39] In this respect, new batches were synthesized at a controlled temperature of 5 °C. The polymerization was performed twice ($PSar_{75}$-*b*-P(LGluOBn$_{46}$-*co*-DGluOBn$_{46}$) (**4a**) and $PSar_{58}$-*b*-P(LGluOBn$_{40}$-*co*-DGluOBn$_{40}$) (**4b**)). The good agreement between ^{1}H NMR and SEC analyses in comparison with theoretical values (**Table 1, Figures S7, S8, S10**) confirms that the desired copolymer was successfully obtained. This also proves the robustness and the repeatability of our polymerization pathway at 5 °C to obtain well-defined $PSar_n$-*b*-P(LGluOBn$_x$-*co*-DGluOBn$_y$) copolymers, even with hydrophobic blocks of rather high molar masses. In the case of $PSar_{70}$-*b*-P(LGluOBn$_{12}$-*co*-DGluOBn$_{12}$), another experiment was performed to check if the polymerization of the PGluOBn block at 5 °C presents any advantage. When compared to $PSar_{70}$-*b*-P(LGluOBn$_{13}$-*co*-DGluOBn$_{13}$) (**3a**), the results obtained for $PSar_{63}$-*b*-P(LGluOBn$_{11}$-*co*-DGluOBn$_{11}$) (**3c**) were not significantly improved (**Table 1**): slightly lower NMR M_n, same *f*, comparable SEC M_n and slightly lower dispersity (1.17 against 1.23) and a slightly better yield (84% against 76%). To conclude, we optimized the synthesis conditions for the polymerization of $PSar_n$-*b*-P(LGluOBn$_x$-*co*-DGluOBn$_y$) with a racemic PGluOBn block. We chose the sequential approach of polymerizing the PGluOBn from a well-defined PSar macroinitiator. Depending on the length of the aimed PGluOBn block, the polymerization temperature was adapted: room temperature gave good results as long as the targeted molar mass was sufficiently low (up to 34 GluOBn repeat units) in the cases of (**1**), (**2**), (**3a**), (**3b**) copolymers); whereas polymerization of the PGluOBn block at 5 °C was necessary when aiming the high molar mass of copolymers (**4a**), (**4b**) (90 GluOBn repeat units).

Table 1. Characteristics of the different $PSar_n$-*b*-P(LGluOBn$_x$-*co*-DGluOBn$_y$) copolymers obtained by polymerization of a racemic PGluOBn block starting from a PSar macroinitiator.

$PSar_n$-*b*-P(LGluOBn$_x$-*co*-DGluOBn$_y$)															
	Targeted[1]							**Obtained**							
								NMR[4]				**SEC[5]**			
Name	**PSar[2]**	**n**	**x**	**y**	**M_n (kg.mol^{-1})**	***f* (%)**	**T[3] (°C)**	**n**	**x + y**	**M_n (kg.mol^{-1})**	***f* (%)**	**M_n (kg.mol^{-1})**	**Đ**	**Yield (%)**
$PSar_{28}$-*b*-P(LGluOBn$_{4.5}$-*co*-DGluOBn$_{4.5}$) (**1**)	S2	28	4.5	4.5	4.0	50	RT	28	9	4.0	50	5.0	1.22	70
$PSar_{28}$-*b*-P(LGluOBn$_{17}$-*co*-DGluOBn$_{17}$) (**2**)	S2	28	18	18	10.0	20	RT	28	33	9.2	21	8.7	1.45	73
$PSar_{70}$-*b*-P(LGluOBn$_{13}$-*co*-DGluOBn$_{13}$) (**3a**)	S1	70	12	12	10.0	50	RT	70	25	10.5	48	9.4	1.23	76
$PSar_{76}$-*b*-P(LGluOBn$_9$-*co*-DGluOBn$_9$) (**3b**)	/	70	12	12	10.0	50	RT	76	18	9.3	58	7.9	1.21	54
$PSar_{63}$-*b*-P(LGluOBn$_{11}$-*co*-DGluOBn$_{11}$) (**3c**)	S1	70	12	12	10.2	50	5	63	22	9.3	48	9.2	1.17	84
$PSar_{75}$-*b*-P(LGluOBn$_{46}$-*co*-DGluOBn$_{46}$) (**4a**)	S1	70	45	45	25.0	20	5	75	91	25.3	21	24.6	1.24	70
$PSar_{58}$-*b*-P(LGluOBn$_{40}$-*co*-DGluOBn$_{40}$) (**4b**)	S1	70	45	45	25.0	20	5	58	79	21.4	19	23.8	1.26	76
$PSar_{76}$-*b*-P(LGluOBn$_{47}$-*co*-DGluOBn$_{47}$) (**4c**)	S1	70	45	45	25.0	20	RT	76	93	25.6	20	18.4	1.34	60

[1] Targeted values are calculated according to n = [Sar NCA]$_0$/[neopentylamine]$_0$ in the PSar macroinitiator synthesis; x = [LGluOBn NCA]$_0$/[PSar]$_0$ and y = [DGluOBn NCA]$_0$/[PSar]$_0$ in the copolymer synthesis using PSar block as macroinitiator

[2] PSar batch used as macroinitiator

/ PSar block intermediate not isolated

[3] Temperature of polymerization of the PGluOBn block

RT: room temperature
[4] Determined by ^{1}H NMR in DMSO-d_6
[5] Determined by SEC in DMF, RI detection, PS calibration

The possibility of polymerizing an enantiomerically pure hydrophobic block was also studied. We decided to focus on the copolymer with a 5.0 kg.mol^{-1} PSar block and a hydrophilic fraction f = 50%, with a PGluOBn block of 23 repeat units and 5.0 kg.mol^{-1}. In a first attempt, the LGluOBn hydrophobic block was polymerized from the **S1** macroinitiator as previously described, both at room temperature (RT) and at 0 °C. The characteristics of these two copolymers are summarized in **Table S2,** ^{1}H NMR spectra and SEC traces are presented in **Figures S11–S13**. The polymerization made at room temperature led to results in good agreement with theoretical values: degree of polymerization of the PSar block n = 66 and degree of polymerization of the PGluOBn block x_{NMR} = 23 according to the ^{1}H NMR spectrum (**Figure S11**) and M_n = 9.8 kg.mol^{-1} with a dispersity of 1.36 by SEC (**Table S2**). However, the RI trace by SEC revealed a bimodal distribution (**Figure S13).** The synthesis performed at 0 °C led to a PLGluOBn block significantly lower than expected (x_{NMR} = 11, when 23 was aimed, **Figure S12**), a copolymer molar mass significantly lower than expected ($M_{n\ SEC}$ = 6.0 kg.mol^{-1}, **Table S2**), and a bimodal RI signal (**Figure S13)**. Such bimodal distributions could either be due to a poor control of the polymerization and/or be the consequence of mixed conformations, as already reported for such low molar masses enantiomerically pure polypeptides.[28,40–42]

Inspired by Barz and coll.[11] work, we also investigated the synthesis of a P(LGluOBn)$_x$-*b*-PSar$_n$ by a so-called "reverse" process to compare both processes. Neopentylamine was used as an initiator and added to the LGluOBn NCA solution in DMF. After the end of the CO_2 release, total consumption of GluOBn NCA was confirmed by FTIR spectroscopy and the Sar NCA was then added to the reaction medium (**Scheme 2**). After total conversion, the copolymer was purified and characterized (PLGluOBn$_{23}$-*b*-PSar$_{80}$ (**5**), **Table 2, Figures 3A, S14**). An aliquot of the reaction medium, after total consumption of GluOBn NCA and before adding Sar NCA, was taken and purified by precipitation in methyl *tert*-butyl ether (MTBE). The superposition of the SEC traces of the aliquot and the final copolymer displays a clear shift, proving a complete initiation of the second block and a good control of the polymerization (**Figure 3A**).

A second analysis by SEC of PLGluOBn$_{23}$-*b*-PSar$_{80}$ (**5**), PSar$_{66}$-*b*-PLGluOBn$_{23}$ and PSar$_{60}$-*b*-PLGluOBn$_{11}$ was performed on a SEC chain with a light scattering (LS) detector (**Figure S15, Table S3**), confirming a monomodal signal for PLGluOBn$_{23}$-*b*-PSar$_{80}$ (**5**) (**Figure S15A**) with a dispersity of 1.28, and bimodal signals for PSar$_{66}$-*b*-PLGluOBn$_{23}$ (**Figure S15B**) and PSar$_{60}$-*b*-PLGluOBn$_{11}$ (**Figure S15C**). The molar mass distributions obtained by LS were linear, the bimodal distributions thus mean that two distinct populations of different molar masses were obtained. SEC does not provide information on whether the two populations have the same conformation or not. To provide another characterization, ^{1}H-DOSY NMR of PSar$_{66}$-*b*-PLGluOBn$_{23}$ was performed in DMSO-d_6 (**Figure S16**). Only one diffusion coefficient was found at 73.5 µm.s^{-1}, significantly lower than 188.4 µm.s^{-1} for the PSar **S1** block (**Figure S17**), indicating that the copolymer was formed. However, some signals were not perfectly aligned (7.4, 5.0 and 2.0 ppm were at a lower diffusion coefficient), and a second signal at a higher diffusion coefficient was detected at 7.4 ppm indicating the presence of impurities in this sample. The nature of these impurities was not investigated. Since the polymerization was performed at RT, it is possible that some pyroglutamate end-group was obtained,[36] and it is also possible that some PSar was not initiated and/or that some PLGluOBn homopolymer was also formed.

Taken together, these results indicate that in our polymerization conditions, the "reverse" process is more controlled than the "normal" process for copolymers with a pure PLGluOBn block. This was not the case for Barz and coll.[11] but their polymerization conditions differ with ours: their Sar NCA undergoes sublimation and polymerization is performed under dried nitrogen. Such drastic conditions might lead to a better control of the polymerization (lower dispersity, lower amount of impurities), but they can't be scaled up for industrial applications. Since we were satisfied with the quality of PLGluOBn$_{23}$-*b*-PSar$_{80}$ (**5**), the "reverse" process was also used to synthesize a copolymer with a pure DGluOBn block. A well-defined PDGluOBn$_{23}$-*b*-PSar$_{70}$ (**7**) was obtained (**Table 2, Figure 3B, S18**). In the case of a racemic mix of LGluOBn NCA and DGluOBn NCA, the copolymer P(LGluOBn$_{13}$-*co*-DGluOBn$_{13}$)-*b*-PSar$_{75}$ (**9**) was obtained (**Table 2, Figures S19, S20**). The NMR results are in good agreement with the theoretical values, but the M_n determined by SEC is much lower than the theoretical value and that the one obtained for the "normal" process (PSar$_{70}$-*b*-P(LGluOBn$_{13}$-*co*-DGluOBn$_{13}$) (**3a**), **Table 1**). Therefore, we considered that the "normal" process was more suitable for the racemic PGluOBn block.

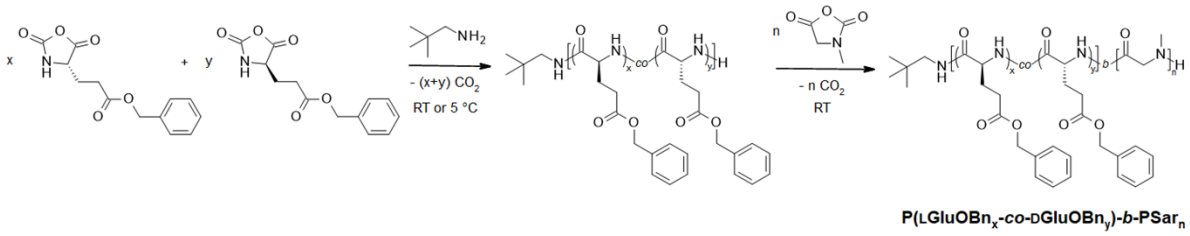

Scheme 2. One-pot synthesis of P(LGluOBn$_x$-*co*-DGluOBn$_y$)-*b*-PSar$_n$ copolymers: ROP of LGluOBn and/or DGluOBn NCAs using neopentylamine as initiator, directly followed by ROP of Sar NCA.

To investigate the influence of the chain-end on the self-assembly, the three reverse copolymers PLGluOBn$_x$-*b*-PSar$_n$, PDGluOBn$_y$-*b*-PSar$_n$ and P(LGluOBn$_x$-*co*-DGluOBn$_y$)-*b*-PSar$_n$ were acetylated using acetic anhydride under basic conditions. The three corresponding functionalized copolymers were isolated and characterized resulting in: PLGluOBn$_{23}$-*b*-PSar$_{80}$-Ac (**6**), PDGluOBn$_{22}$-*b*-PSar$_{68}$-Ac (**8**), and P(LGluOBn$_{11}$-*co*-DGluOBn$_{11}$)-*b*-PSar$_{68}$-Ac (**10**) (**Table 2**). The methyl protons of the acetyl end-group were not identifiable as they are assumed to resonate at around 2.0 ppm and are most likely hidden under the methylene signals of the GluOBn moieties (2.1 – 1.5 ppm). ^{1}H NMR spectra are presented in **Figures S21–S23**. However, the slight increase in M_n by SEC (**Table 2**, **Figure 3**) while the M_n and *f* calculated by ^{1}H NMR are constant, is consistent with an effective acetylation of the copolymers.

Table 2. Characteristics of the different P(LGluOBn$_x$-*co*-DGluOBn$_y$)-*b*-PSar$_n$ copolymers obtained by a one-pot polymerization of the PGluOBn block followed by the PSar block and an optionnal acetylation.

P(LGluOBn$_x$-*co*-DGluOBn$_y$)-*b*-PSar$_n$														
	Targeted[1]						Obtained							
							NMR[3]				SEC[4]			
Name	x	y	n	M_n (kg.mol^{-1})	*f* (%)	T[2] (°C)	x + y	n	M_n (kg.mol^{-1})	*f* (%)	M_n (kg.mol^{-1})	Đ	Yield (%)	
PLGluOBn$_{23}$-*b*-PSar$_{80}$ (**5**)	23	0	70	10.0	50	RT	23	80	10.8	53	10.1	1.22	91	
PLGluOBn$_{23}$-*b*-PSar$_{80}$-Ac (**6**)	23	0	70	10.0	50	RT	23	80	10.8	53	11.4	1.19	77*	
PDGluOBn$_{23}$-*b*-PSar$_{70}$ (**7**)	0	23	70	10.0	50	5	23	70	10.0	50	9.9	1.11	84	
PDGluOBn$_{22}$-*b*-PSar$_{68}$-Ac (**8**)	0	23	70	10.0	50	5	22	68	9.7	50	10.6	1.09	69*	
P(LGluOBn$_{13}$-*co*-DGluOBn$_{13}$)-*b*-PSar$_{75}$ (**9**)	12	12	70	10.2	49	RT	25	75	10.7	50	7.0	1.38	89	
P(LGluOBn$_{11}$-*co*-DGluOBn$_{11}$)-*b*-PSar$_{68}$-Ac (**10**)	12	12	70	10.2	49	RT	22	68	9.7	50	8.2	1.23	77*	

[1] Targeted values are calculated according to x = n[LGluOBn NCA]$_0$ /n[neopentylamine]$_0$ and y = n[DGluOBn NCA]$_0$ /n[neopentylamine]$_0$ and n = n[Sar NCA]$_0$ /n[neopentylamine]$_0$ in the copolymer synthesis using neopentylamine as initiator
[2] Temperature of polymerization of the PGluOBn block
RT: room temperature
[3] Determined by ^{1}H NMR in DMSO-d_6
[4] Determined by SEC in DMF, RI detection, PS calibration
* Overall yield from the copolymer synthesis to the capping step for the acetylated copolymers (P(LGluOBn$_x$-*co*-DGluOBn$_y$)-*b*-PSar$_n$-Ac).

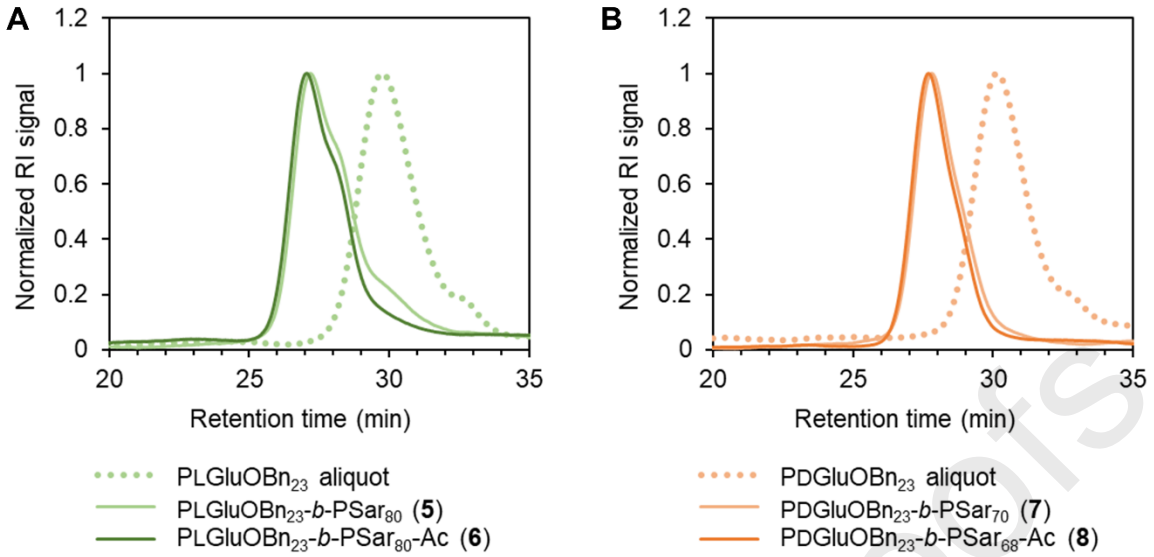

Figure 3. SEC traces (DMF, RI detection) of: A) the PLGluOBn first block aliquot, PLGluOBn$_x$-*b*-PSar$_n$, and PLGluOBn$_x$-*b*-PSar$_n$-Ac and B) the PDGluOBn first block aliquot, PDGluOBn$_x$-*b*-PSar$_n$, and PDGluOBn$_x$-*b*-PSar$_n$-Ac.

In the objective to better understand the secondary structures that could be involved, all copolymers were analyzed in solid form by FTIR spectroscopy (spectra in **Figures S24–S37**). As expected, copolymers containing an enantiomerically pure PGluOBn block (PLGluOBn or PDGluOBn) present wavelength values for the amide CO stretching I and II that may correspond to an α-helix secondary structure[43,44] (**Table S4**). Sill and coll.[29] established through circular dichroism spectroscopy that PEG$_{273}$-*b*-PLGluOBn$_{30}$-Ac presented a helical secondary structure whereas its « D/L-isomer mixture counterpart » PEG$_{273}$-*b*-P(LGluOBn$_{15}$-*co*-DGluOBn$_{15}$)-Ac presented a random coil secondary structure. On the contrary, in the case of copolymers we synthesized in this work with a racemic PGluOBn block, the values of amide CO stretching I and II seem to correspond to α-helix secondary structures (**Table S5**). The differences observed with previous work might be explained by the nature of our system itself which is significantly different from the one mentioned above: nature of the hydrophilic block (PSar instead of PEG), size of the hydrophilic block (PSar of 2 or 5 kg.mol^{-1} instead of PEG of 12 kg.mol^{-1}) resulting in less hydrophilic copolymers.

Finally, we have optimized the synthesis conditions for the different targeted copolymers. With racemic P(LGluOBn-*co*-DGluOBn) hydrophobic block, four copolymers with a hydrophilic PSar block of 2 or 5 kg.mol^{-1} and a hydrophilic weight fraction of 20 or 50% were successfully synthesized and characterized. Furthermore, two additional copolymers were obtained by varying the nature of the hydrophobic block: pure L or pure D, using a so-called “reverse” process. For this purpose, the 5 kg.mol^{-1} hydrophilic PSar block with a 50% hydrophilic fraction design was selected. We evidenced that the “reverse” process allowed a better control of the polymerization of the PLGluOBn block, while the “normal” process was more suitable for the copolymer with the racemic P(LGluOBn-*co*-DGluOBn) block. The copolymers obtained by the reverse process are available in two forms depending of the chain-end nature: NH terminated or capped with an acetyl function. The ability of this series of copolymers to self-assemble and load paclitaxel was then studied.

3.2 Formulation of paclitaxel-loaded nanoparticles

Amphiphilic diblock copolymers like our PSar-*b*-PGluOBn can self-assemble in water into nano-sized aggregates when used above their CMC.[10,45–47] Different morphologies can be obtained according to the copolymer’s nature and hydrophilic fraction. This assembly is mainly caused by the hydrophobic effect between the hydrophobic core-forming chains: they tend to associate in order to minimize unfavorable contacts with water molecules. As for the hydrophilic chains, they tend both: to converge to limit the interactions between hydrophobic chains and water molecules, and also to distance themselves due to steric and electrostatic repulsions. Hydrophobic molecules of low molar mass can be physically entrapped in the core of the micelles during the self-assembly.[45,47] The solubilization process is mainly due to hydrophobic interactions between the hydrophobic molecule and the hydrophobic core of the micelles. A scheme of the formation of our nanoparticles is presented in the Figure 4.

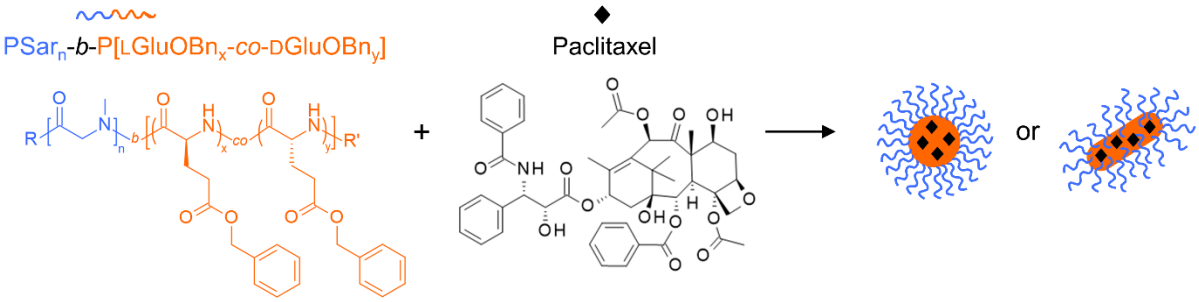

Figure 4. Representative scheme of the formation of PTX-loaded nanoparticles based on our PSar-*b*-PGluOBn copolymers.

Different formulation techniques can be used to form such drug-loaded polymer nanoparticles.[45,47] A nanoprecipitation process was reported for PEG-*b*-PLGluOBn copolymers using a mixture of DMF and tetrahydrofuran (THF) (3/7, v/v),[20] pure THF,[25,26] or dimethyl sulfoxide (DMSO).[11,27,28] For PSar-*b*-PLGluOBn copolymers, Barz *et al.* reported a nanoprecipitation method,[11] dialysis method,[48] and a centrifugation technique.[49] Since paclitaxel and the different PSar-*b*-PGluOBn copolymers described above were all soluble in pure DMF, we decided to perform a nanoprecipitation procedure similar to the literature,[11] in which a solution of copolymer and paclitaxel in DMF at a feed weight ratio of 10% is injected into water in conditions well-above their CMC (**Figure S38**). The obtained NPs were purified by syringe filtration at 0.2 µm and gel filtration chromatography in phosphate buffer saline (PBS) to remove unloaded drug and DMF, while recovering the NPs in PBS, a frequently used aqueous buffer needed to ensure physiological pH and osmolarity required for biological applications.

DLS measurements were performed to measure the hydrodynamic diameter (D_h) of the NPs and their polydispersity index (PDI). Zeta-potential (ZP) measurements were performed to evaluate the surface charge of the NPs. The PTX concentration in the nanoparticles ($[PTX]_{NPs}$) was determined by UPLC (**Figures S39–S42**) and used to evaluate PTX loading efficiency (LE). The copolymer concentration in the nanoparticles ($[C]_{NPs}$) was measured by SEC (**Figures S43–S52**) and used to determine copolymer recovery (CR) and drug loading content (DLC). Finally, the residual DMF content was determined by HS-GC. Results from these characterizations are summarized in **Table 3** and show that all suspensions indeed contained nano-sized particles successfully loaded with paclitaxel. Morphology of the NPs was also investigated by cryo-TEM (**Figures 5, 6, S53**).

The NPs' size and size distribution varied according to the copolymer used in the nanoprecipitation. All NPs had a size below 200 nm, which is preferred for passive targeting applications. For PSar$_n$-*b*-P(LGluOBn$_x$-*co*-DGluOBn$_y$) copolymers with a racemic PGluOBn block, whether the PSar molar mass was 2 or 5 kg.mol^{-1}, a hydrophilic fraction of 20% gave larger NPs than 50% with 27 and 22 nm for PSar$_{28}$-*b*-P(LGluOBn$_{4.5}$-*co*-DGluOBn$_{4.5}$) (**1**) and PSar$_{28}$-*b*-P(LGluOBn$_{17}$-*co*-DGluOBn$_{17}$) (**2**) (**Figure 5**) versus 109 and 83 nm for PSar$_{63}$-*b*-P(LGluOBn$_{11}$-*co*-DGluOBn$_{11}$) (**3c**) and PSar$_{58}$-*b*-P(LGluOBn$_{40}$-*co*-DGluOBn$_{40}$) (**4b**) (**Figure 5B**), respectively. Cryo-TEM confirmed a difference in size between samples (**Figure 5C–F**). PSar$_{28}$-*b*-P(LGluOBn$_{4.5}$-*co*-DGluOBn$_{4.5}$) (**1**) and PSar$_{28}$-*b*-P(LGluOBn$_{17}$-*co*-DGluOBn$_{17}$) (**2**) NPs were a mix of different structures: small spherical particles, small elongated particles, cylindrical particles, and large spherical particles for PSar$_{28}$-*b*-P(LGluOBn$_{17}$-*co*-DGluOBn$_{17}$) (**2**) sample. Whereas cryo-TEM of PSar$_{63}$-*b*-P(LGluOBn$_{11}$-*co*-DGluOBn$_{11}$) (**3c**) only showed spherical particles and PSar$_{58}$-*b*-P(LGluOBn$_{40}$-*co*-DGluOBn$_{40}$) (**4b**) a mix of spherical and elongated particles. It is possible that the better homogeneity of morphologies of the PSar$_{63}$-*b*-P(LGluOBn$_{11}$-*co*-DGluOBn$_{11}$) (**3c**) and PSar$_{58}$-*b*-P(LGluOBn$_{40}$-*co*-DGluOBn$_{40}$) (**4b**) samples compared to the PSar$_{28}$-*b*-P(LGluOBn$_{4.5}$-*co*-DGluOBn$_{4.5}$) (**1**) and PSar$_{28}$-*b*-P(LGluOBn$_{17}$-*co*-DGluOBn$_{17}$) (**2**) samples is due to their higher molar masses (PSar of 5 kg.mol^{-1} versus 2 kg.mol^{-1}), but since the temperature of synthesis was not the same (5 °C versus RT), this also might have impacted the L/D amino acid sequence arrangement given that FTIR data showed α-helix structures for all our copolymers. The presence of elongated particles for the PSar$_{58}$-*b*-P(LGluOBn$_{40}$-*co*-DGluOBn$_{40}$) (**4b**) sample (*f* = 20%, longer PGluOBn block) compared to PSar$_{63}$-*b*-P(LGluOBn$_{11}$-*co*-DGluOBn$_{11}$) (**3c**) NPs (*f* = 50%), was not particularly expected since kinetically trapped structures were assumed due to the rapid nanoprecipitation technique that was chosen, so the resulting morphology was not necessarily the one obtained at the thermodynamic equilibrium. In the literature, elongated nanoparticles have been reported for the enantiomerically pure PLGluOBn polymer,[26,50] with a larger aspect ratio for higher molar masses of PLGluOBn,[50] which is consistent with our findings.

Zeta-potential of NPs formed with the four $PSar_n$-*b*-P(LGluOBn$_x$-*co*-DGluOBn$_y$) copolymers with a racemic PGluOBn block, were all slightly negative with values between –6 and –18 mV (**Table 3**). Interestingly, the lowest ZPs were obtained for the copolymers with *f* = 20% ($PSar_{28}$-*b*-P(LGluOBn$_{17}$-*co*-DGluOBn$_{17}$) (**2**) and $PSar_{58}$-*b*-P(LGluOBn$_{40}$-*co*-DGluOBn$_{40}$) (**4b**)) and there was no correlation between ZP and PSar block length. Since paclitaxel was also loaded in the NPs, it is possible that some of the PTX was absorbed on the surface of the NPs and impacted the apparent ZP.

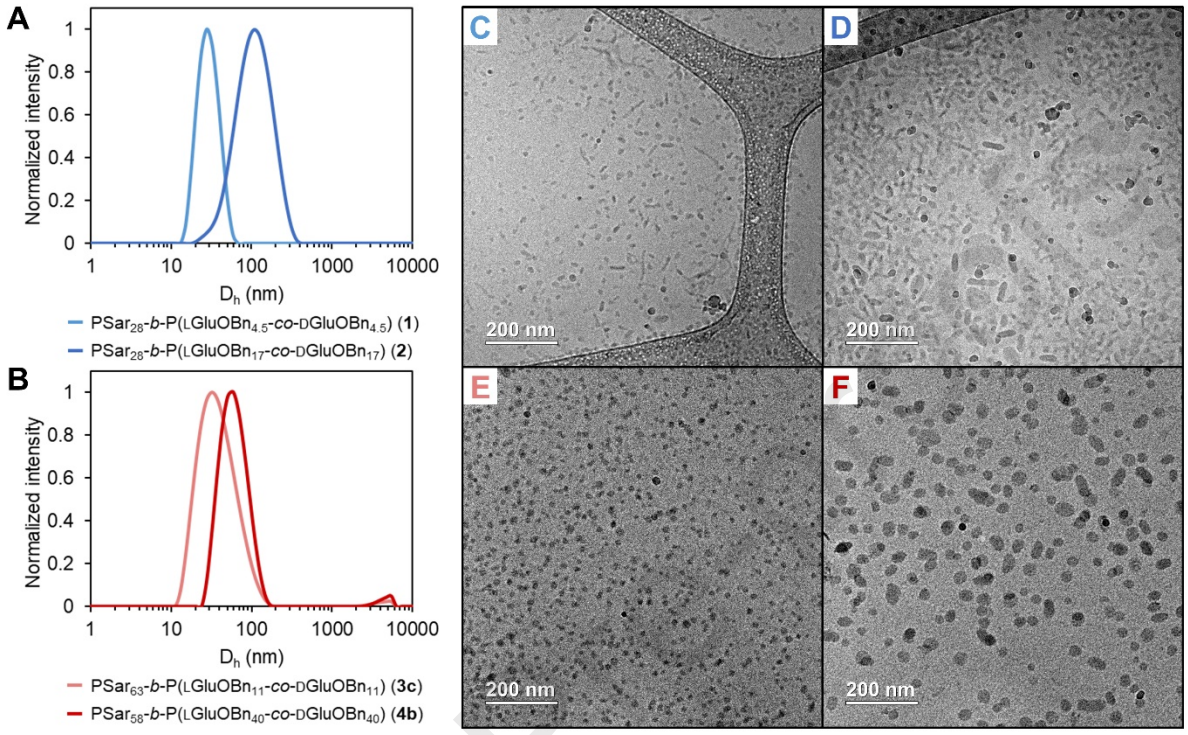

Figure 5. A, B) Size distribution by DLS, and C – F) cryo-TEM pictures of paclitaxel-loaded nanoparticles in PBS formed with: $PSar_{28}$-*b*-P(LGluOBn$_{4.5}$-*co*-DGluOBn$_{4.5}$) (**1**) (A light blue, C), $PSar_{28}$-*b*-P(LGluOBn$_{17}$-*co*-DGluOBn$_{17}$) (**2**) (A dark blue, D), $PSar_{63}$-*b*-P(LGluOBn$_{11}$-*co*-DGluOBn$_{11}$) (**3c**) (B light red, E), and $PSar_{58}$-*b*-P(LGluOBn$_{40}$-*co*-DGluOBn$_{40}$) (**4b**) (B dark red, F).

For PLGluOBn$_x$-*b*-$PSar_n$ and PDGluOBn$_y$-*b*-$PSar_n$ copolymers and their acetylated version, the four types of NPs were all small and well-defined with D_h between 27 and 31 nm and PDI between 0.01 and 0.06 (**Figure 6A, B** and **Table 3**). Cryo-TEM images showed that PLGluOBn$_{23}$-*b*-$PSar_{80}$ (**5**), PLGluOBn$_{23}$-*b*-$PSar_{80}$-Ac (**6**) and PDGluOBn$_{22}$-*b*-$PSar_{68}$-Ac (**8**) NPs were a mix of small spherical and elongated particles and longer cylindrical particles (**Figure 6C, D, F** respectively) and PDGluOBn$_{23}$-*b*-$PSar_{70}$ (**7**) NPs were a mix of particulates and small elongated particles (**Figure 6E**). The elongated particles and cylindrical particles are more present for these PLGluOBn$_x$-*b*-$PSar_n$ and PDGluOBn$_y$-*b*-$PSar_n$ copolymers made of enantiomerically pure hydrophobic blocks compared to the $PSar_n$-*b*-P(LGluOBn$_x$-*co*-DGluOBn$_y$) copolymers composed of a racemic hydrophobic block for a 5 kg.mol^{-1} PSar. The particulate morphology was already reported for a PEG-*b*-PLGluOBn system,[27] but to the best of our knowledge, no one had yet reported a self-assembly study on a PDGluOBn system including PDGluOBn-*b*-PSar. Zeta-potential of NPs was slightly positive for PLGluOBn$_{23}$-*b*-$PSar_{80}$ (**5**), and PDGluOBn$_{23}$-*b*-$PSar_{70}$ (**7**) (+3 mV and +21 mV respectively) and slightly negative for their acetylated counterparts PLGluOBn$_{23}$-*b*-$PSar_{80}$-Ac (**6**) and PDGluOBn$_{22}$-*b*-$PSar_{68}$-Ac (**8**) (–10 mV and –5 mV respectively) indicating that capping with an acetyl group contributes to decreasing the surface charge of the NPs, which is consistent with a previous report indicating an enhanced stealthiness of polysarcosine through acetylation.[51]

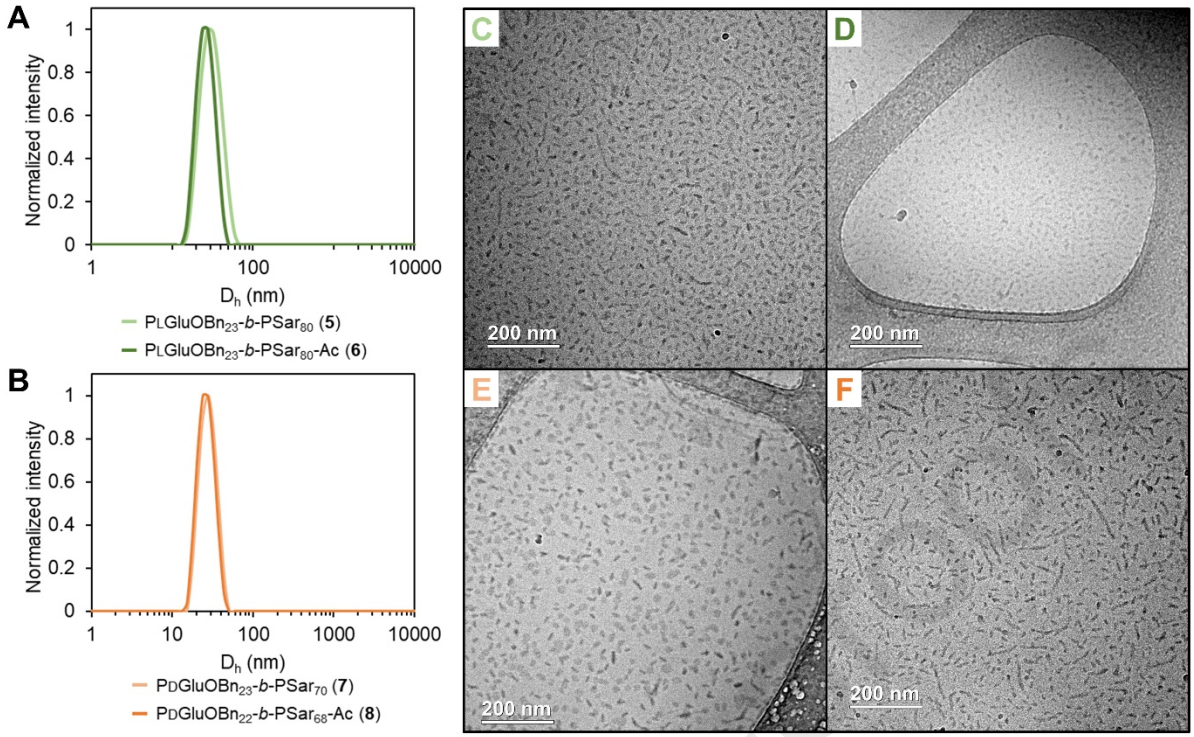

Figure 6. A, B) Size distribution by DLS, and C – F) cryo-TEM pictures of paclitaxel-loaded nanoparticles in PBS formed with: PLGluOBn$_{23}$-*b*-PSar$_{80}$ (**5**) (A light green, C), PLGluOBn$_{23}$-*b*-PSar$_{80}$-Ac (**6**) (A dark green, D), PDGluOBn$_{23}$-*b*-PSar$_{70}$ (**7**) (B light orange, E), and PDGluOBn$_{22}$-*b*-PSar$_{68}$-Ac (**8**) (B dark orange, F).

In additional experiments, P(LGluOBn$_{13}$-*co*-DGluOBn$_{13}$)-*b*-PSar$_{75}$ (**9**) and P(LGluOBn$_{11}$-*co*-DGluOBn$_{11}$)-*b*-PSar$_{68}$-Ac (**10**) were also formulated with paclitaxel and characterized (**Table S6**, **Figure S53**). The size of P(LGluOBn$_{13}$-*co*-DGluOBn$_{13}$)-*b*-PSar$_{75}$ (**9**) NPs was similar to the PLGluOBn$_{23}$-*b*-PSar$_{80}$ (**5**) and PDGluOBn$_{23}$-*b*-PSar$_{70}$ (**7**) NPs with D_h = 31 nm (PDI = 0.01, **Figure S53A**). P(LGluOBn$_{11}$-*co*-DGluOBn$_{11}$)-*b*-PSar$_{68}$-Ac (**10**) NPs were bigger with D_h = 57 nm (PDI = 0.11). The size increase was not observed for the PLGluOBn$_{23}$-*b*-PSar$_{80}$-Ac (**6**) and PDGluOBn$_{22}$-*b*-PSar$_{68}$-Ac (**8**) NPs. Cryo-TEM images showed a mixture of small elongated particles, spherical objects that seem to be vesicles for P(LGluOBn$_{13}$-*co*-DGluOBn$_{13}$)-*b*-PSar$_{75}$ (**9**) NPs (**Figure S53B**), and small elongated particles and particulates and/or vesicles for P(LGluOBn$_{11}$-*co*-DGluOBn$_{11}$)-*b*-PSar$_{68}$-Ac (**10**) (**Figure S53C**), and not spherical nanoparticles like for PSar$_{63}$-*b*-P(LGluOBn$_{11}$-*co*-DGluOBn$_{11}$) (**3c**) NPs (**Figure 5E**). Since P(LGluOBn$_{13}$-*co*-DGluOBn$_{13}$)-*b*-PSar$_{75}$ (**9**) was synthesized at RT, it is again possible that the L/D amino acid sequence in the racemic block is different between P(LGluOBn$_{13}$-*co*-DGluOBn$_{13}$)-*b*-PSar$_{75}$ (**9**) and PSar$_{63}$-*b*-P(LGluOBn$_{11}$-*co*-DGluOBn$_{11}$) (**3c**). The zeta-potential was slightly lower for P(LGluOBn$_{11}$-*co*-DGluOBn$_{11}$)-*b*-PSar$_{68}$-Ac (**10**) NPs compared to P(LGluOBn$_{13}$-*co*-DGluOBn$_{13}$)-*b*-PSar$_{75}$ (**9**) NPs, consistent with what was observed for the PLGluOBn$_x$-*b*-PSar$_n$ and PDGluOBn$_y$-*b*-PSar$_n$ NPs and their acetylated version.

Overall, on the ten different copolymer NPs obtained, paclitaxel loading was similar between samples with PTX concentration ranging from 0.39 to 0.58 g.L^{-1} and LE from 63 to 84% (**Tables 3**, **S6**). It should be noted that the samples were diluted during the gel filtration chromatography, as expected, but with a slight difference in dilution factors (DF = 1.2 – 1.6) due to manual fraction collection, which resulted in the discrepancy between [PTX] and LE, when for example a [PTX] of 0.73 g.L^{-1} could have been expected for a LE of 73%, while 0.55 g.L^{-1} was obtained (DF = 1.3 for PSar$_{28}$-*b*-P(LGluOBn$_{4.5}$-*co*-DGluOBn$_{4.5}$) (**1**) NPs). PTX apparent solubility in aqueous buffer was thus significantly improved using PSar-*b*-PGluOBn NPs with up to 580 µg.mL^{-1}, compared to less than 0.1 µg.mL^{-1} for free PTX according to the litterature,[52] hence an apparent solubility increase of a factor 5800. We also performed a control experiment using the same nanoprecipitation procedure and only PTX (without polymer). PTX precipitated during the addition of the PTX solution in DMF into water. After filtration through 0.2 µm, only 0.014 g.L^{-1} (14 µg.mL^{-1}) of [PTX] was obtained in the H_2O/DMF mixture at 9/1 v/v. No further purification by gel filtration chromatography in PBS was performed at the risk of being close to the limit of detection of our method (0.2 µg.mL^{-1}), but this experiment further proved the benefit of our copolymers.

The copolymer concentration in NPs was ranging from 2.8 to 6.9 $g.L^{-1}$, copolymer recovery from 34 to 91%, and drug loading contents from 7 to 15% (**Tables 3**, **S6**). The $PLGluOBn_x$-*b*-$PSar_n$ and $PDGluOBn_y$-*b*-$PSar_n$ copolymer NPs and their acetylated version (**5–8**) exhibited low CR, resulting in DLC higher than theoretically possible (9%). This could be due to the loss of polymer during the different purification steps, especially since only the PTX-concentrated fractions were combined after the gel filtration column to maximize $[PTX]_{NPs}$. Another reason might be that polymer loss occurred during sample preparation for analysis by SEC. Indeed, since the salts in PBS are not fully soluble in DMF LiBr, the filtration of the samples before injection into the SEC system may have removed a fraction of the polymer in addition to the salts.

Advantageously, all nanoparticles had low traces of DMF (< 38 ppm, **Tables 3**, **S6**), well below the acceptable limit of 880 ppm for pharmaceuticals according to the international conference harmonization guidelines,[53] further proving that paclitaxel was only solubilized in PBS due to self-assembly of the PSar-*b*-PGluOBn copolymers. Colloidal stability of the nanoparticles was investigated upon storage at 4 °C and after one freeze-thaw cycle (**Table S7**). After storage for 8 to 12 days at 4 °C, nanoparticles of (**4b**), (**5**), (**7**) and (**8**) were all stable. After one freeze-thaw cycle, NPs of (**1**) to (**8**) were all fairly stable. More precisely, NPs of (**5**) and (**7**) were less stable than NPs of (**6**) and (**8**), showing the advantage of acetylation.

Table 3. Characteristics of paclitaxel-loaded nanoparticles in PBS formed with the different PSar-*b*-PGluOBn copolymers using the same nanoprecipitation conditions: D_h, PDI, ZP, DF, $[PTX]_{NPs}$, LE, $[C]_{NPs}$, CR, DLC, DMF content.

	DLS		ZP			UPLC		SEC			HS-GC
Copolymer	**D_h (nm)**	**PDI**	**ZP (mV)**	**ZP derivation (mV)**	**DF**	**$[PTX]_{NPs}$ ($g.L^{-1}$)**	**LE (%)**	**$[C]_{NPs}$ ($g.L^{-1}$)**	**CR (%)**	**DLC (%)**	**DMF content (ppm)**
$PSar_{28}$-*b*-P($LGluOBn_{4.5}$-*co*-$DGluOBn_{4.5}$) (**1**)	30	0.08	–6 ± 2	5 ± 2	1.3	0.55	73%	6.9	91%	7%	22
$PSar_{28}$-*b*-P($LGluOBn_{17}$-*co*-$DGluOBn_{17}$) (**2**)	118	0.20	–23 ± 2	12 ± 5	1.6	0.39	63%	4.7	75%	8%	15
$PSar_{63}$-*b*-P($LGluOBn_{11}$-*co*-$DGluOBn_{11}$) (**3c**)	42	0.20	–10 ± 2	17 ± 6	1.4	0.58	83%	5.6	80%	9%	16
$PSar_{58}$-*b*-P($LGluOBn_{40}$-*co*-$DGluOBn_{40}$) (**4b**)	63	0.17	–15 ± 5	13 ± 6	1.5	0.55	80%	5.9	86%	8%	24
$PLGluOBn_{23}$-*b*-$PSar_{80}$ (**5**)	31	0.06	3 ± 2	4 ± 1	1.5	0.57	84%	4.3	63%	12%	17
$PLGluOBn_{23}$-*b*-$PSar_{80}$-Ac (**6**)	27	0.03	–10 ± 1	8 ± 4	1.2	0.51	62%	2.8	34%	15%	23
$PDGluOBn_{23}$-*b*-$PSar_{70}$ (**7**)	28	0.01	21 ± 1	3 ± 1	1.5	0.56	83%	4.1	60%	12%	32
$PDGluOBn_{22}$-*b*-$PSar_{68}$-Ac (**8**)	27	0.02	–5 ± 4	12 ± 4	1.5	0.52	78%	3.1	46%	15%	18

To conclude, for hydrophilic fraction of 50%, the $PSar_{63}$-*b*-P($LGluOBn_{11}$-*co*-$DGluOBn_{11}$) (**3c**) NPs (racemic PGluOBn block synthesized at 5 °C in a two-step process starting with PSar 5 $kg.mol^{-1}$) are the most well-defined NPs with a spherical morphology. $PLGluOBn_x$-*b*-$PSar_n$ and $PDGluOBn_y$-*b*-$PSar_n$ copolymers, especially after acetylation, are of interest since they are smaller and still have high paclitaxel loaded concentrations. For a hydrophilic fraction of 20%, $PSar_{58}$-*b*-P($LGluOBn_{40}$-*co*-$DGluOBn_{40}$) (**4b**) NPs (PSar 5 $kg.mol^{-1}$, synthesized at 5 °C) performed better than $PSar_{28}$-*b*-P($LGluOBn_{17}$-*co*-$DGluOBn_{17}$) (**2**) NPs (PSar 2 $kg.mol^{-1}$, synthesized at RT), especially since NPs were more homogeneous in size and morphology, had the lowest zeta-potential, and one of the highest loading efficiencies among the ten obtained NPs.

Finally, a screening of the formulation conditions (FWR and FR) was performed with $PSar_{58}$-*b*-P($LGluOBn_{40}$-*co*-$DGluOBn_{40}$) (**4b**) by adapting our formulation procedure (**Table S8**). For FWR 5%, the NPs size right after nanoprecipitation decreased when increasing the FR, a trend that can be expected when forcing a rapid self-assembly, but the NPs size after purification was very similar around 45 nm. LE were higher than 73% for the three FR. For FWR 10%, no impact on the nanoparticle size was observed after nanoprecipitation, which might be explained by the impact of a higher LE and $[PTX]_{NPs}$ on the NPs size, compared to FWR 5%. For FWR 20%, samples were opaque after nanoprecipitation, LE was lower than 46% and visible precipitates were observed after storage one day at 4 °C, meaning that this FWR was too high in these conditions. The best condition was a FWR of 10% and FR of 1 $mL.min^{-1}$ that led to NPs of 44 nm in diameter, with a PDI of 0.04, a LE of 92% and a $[PTX]_{NPs}$ of 0.66 $g.L^{-1}$, the highest LE and PTX concentrations of this entire work.

4 Conclusions

In order to study the influence of parameters such as hydrophilic fraction, molar mass, nature of the hydrophobic block (racemic, pure L or pure D) on the formulation process and drug loading efficiency, we synthesized different polysarcosine-*block*-poly(benzyl glutamate) PSar-*b*-PGluOBn amphiphilic copolymers. We have optimized the polymerization conditions while maintaining industrially compatible process by varying the polymerization temperature of the PGluOBn block and the sequence of polymerization of the blocks. Indeed, the polymerization of the racemic P(LGluOBn-*co*-DGluOBn) block was controlled starting with a PSar macroinitiator, taking care to perform it at 5 °C for a long block of 90 repeat units. As a result, four copolymers containing racemic PGluOBn block were successfully obtained and characterized with a PSar block of 2 or 5 kg.mol^{-1} of molar mass and a hydrophilic fraction of 20 or 50%. PLGluOBn$_x$-*b*-PSar$_n$ and PDGluOBn$_y$-*b*-PSar$_n$ copolymers with an enantiomerically pure PGluOBn block were also successfully obtained by using a so-called “reverse” process as well as corresponding acetylated copolymers.

Ten different nanoparticles based on ten PSar-*b*-PGluOBn copolymers were formed by the same nanoprecipitation technique and were extensively characterized. All copolymer nanoparticles were shown to be successfully loaded with paclitaxel, a hydrophobic drug model, proving that PSar-*b*-PGluOBn are interesting excipients that can be used to increase the apparent solubility in water of paclitaxel up to 6600 times. Nanoparticles based on the two copolymers PSar$_{63}$-*b*-P(LGluOBn$_{11}$-*co*-DGluOBn$_{11}$) (**3c**) and PSar$_{58}$-*b*-P(LGluOBn$_{40}$-*co*-DGluOBn$_{40}$) (**4b**) with a racemic hydrophobic block synthesized at 5 °C stand out in shape since they are respectively homogeneous spherical and elongated nanoparticles and possess a high loading efficiency and copolymer recovery. Nanoparticles based on PLGluOBn$_{23}$-*b*-PSar$_{80}$-Ac (**6**) and PDGluOBn$_{22}$-*b*-PSar$_{68}$-Ac (**8**) can also be of interest as nanoparticles of smaller size and of a different nature of PGluOBn block (pure L or pure D). The therapeutic potential of our paclitaxel-loaded PSar-*b*-PGluOBn nanoparticles against cancer could be investigated in future experiments.

5 Acknowledgments

This work benefited from the facilities and expertise of the « Mass spectrometry team research » (Vincent Guérineau), Institut de Chimie des Substances Naturelles (ICSN), CNRS, 91198, Gif-sur-Yvette, France. This work also received the expertise of the Transmission Electron Microscopy platform (Jean-Michel Guigner), Institut de Minéralogie, de Physique des Matériaux et de Cosmochimie (IMPMC), Sorbonne Université, CNRS UMR 7590, Muséum National d'Histoire Naturelle, 75005 Paris, France, and of the Chromatography platform at LCPO, CNRS UMR 5629, with the support of Amélie Vax.

6 References

(1) Kalepu, S.; Nekkanti, V. Insoluble Drug Delivery Strategies: Review of Recent Advances and Business Prospects. *Acta Pharm. Sin. B* **2015**, *5* (5), 442–453. https://doi.org/10.1016/j.apsb.2015.07.003.

(2) Singla, A. K.; Garg, A.; Aggarwal, D. Paclitaxel and Its Formulations. *Int. J. Pharm.* **2002**, *235* (1), 179–192. https://doi.org/10.1016/S0378-5173(01)00986-3.

(3) Gelderblom, H.; Verweij, J.; Nooter, K.; Sparreboom, A. Cremophor EL: The Drawbacks and Advantages of Vehicle Selection for Drug Formulation. *Eur. J. Cancer* **2001**, *37* (13), 1590–1598. https://doi.org/10.1016/S0959-8049(01)00171-X.

(4) Wang, F.; Porter, M.; Konstantopoulos, A.; Zhang, P.; Cui, H. Preclinical Development of Drug Delivery Systems for Paclitaxel-Based Cancer Chemotherapy. *J. Control. Release* **2017**, *267*, 100–118. https://doi.org/10.1016/j.jconrel.2017.09.026.

(5) Anselmo, A. C.; Mitragotri, S. Nanoparticles in the Clinic: An Update. *Bioeng. Transl. Med.* **2019**, *4* (3), e10143. https://doi.org/10.1002/btm2.10143.

(6) Peer, D.; Karp, J. M.; Hong, S.; Farokhzad, O. C.; Margalit, R.; Langer, R. Nanocarriers as an Emerging Platform for Cancer Therapy. *Nat. Nanotechnol.* **2007**, *2* (12), 751–760. https://doi.org/10.1038/nnano.2007.387.

(7) Shi, J.; Kantoff, P. W.; Wooster, R.; Farokhzad, O. C. Cancer Nanomedicine: Progress, Challenges and Opportunities. *Nat. Rev. Cancer* **2017**, *17* (1), 20–37. https://doi.org/10.1038/nrc.2016.108.

(8) Wolfram, J.; Ferrari, M. Clinical Cancer Nanomedicine. *Nano Today* **2019**, *25*, 85–98. https://doi.org/10.1016/j.nantod.2019.02.005.
(9) Mitchell, M. J.; Billingsley, M. M.; Haley, R. M.; Wechsler, M. E.; Peppas, N. A.; Langer, R. Engineering Precision Nanoparticles for Drug Delivery. *Nat. Rev. Drug Discov.* **2021**, *20* (2), 101–124. https://doi.org/10.1038/s41573-020-0090-8.
(10) Cabral, H.; Miyata, K.; Osada, K.; Kataoka, K. Block Copolymer Micelles in Nanomedicine Applications. *Chem. Rev.* **2018**, *118* (14), 6844–6892. https://doi.org/10.1021/acs.chemrev.8b00199.
(11) Birke, A.; Huesmann, D.; Kelsch, A.; Weilbächer, M.; Xie, J.; Bros, M.; Bopp, T.; Becker, C.; Landfester, K.; Barz, M. Polypeptoid-Block-Polypeptide Copolymers: Synthesis, Characterization, and Application of Amphiphilic Block Copolypept(o)Ides in Drug Formulations and Miniemulsion Techniques. *Biomacromolecules* **2014**, *15* (2), 548–557. https://doi.org/10.1021/bm401542z.
(12) Klinker, K.; Barz, M. Polypept(o)Ides: Hybrid Systems Based on Polypeptides and Polypeptoids. *Macromolecular Rapid Communications* **2015**, *36* (22), 1943–1957. https://doi.org/10.1002/marc.201500403.
(13) Skoulas, D.; Christakopoulos, P.; Stavroulaki, D.; Santorinaios, K.; Athanasiou, V.; Iatrou, H. Micelles Formed by Polypeptide Containing Polymers Synthesized Via N-Carboxy Anhydrides and Their Application for Cancer Treatment. *Polymers* **2017**, *9* (12), 208. https://doi.org/10.3390/polym9060208.
(14) Sun, H.; Gu, X.; Zhang, Q.; Xu, H.; Zhong, Z.; Deng, C. Cancer Nanomedicines Based on Synthetic Polypeptides. *Biomacromolecules* **2019**, *20* (12), 4299–4311. https://doi.org/10.1021/acs.biomac.9b01291.
(15) Hamaguchi, T.; Matsumura, Y.; Suzuki, M.; Shimizu, K.; Goda, R.; Nakamura, I.; Nakatomi, I.; Yokoyama, M.; Kataoka, K.; Kakizoe, T. NK105, a Paclitaxel-Incorporating Micellar Nanoparticle Formulation, Can Extend in Vivo Antitumour Activity and Reduce the Neurotoxicity of Paclitaxel. *Br. J. Cancer* **2005**, *92* (7), 1240–1246. https://doi.org/10.1038/sj.bjc.6602479.
(16) Song, W.; Tang, Z.; Li, M.; Lv, S.; Sun, H.; Deng, M.; Liu, H.; Chen, X. Polypeptide-Based Combination of Paclitaxel and Cisplatin for Enhanced Chemotherapy Efficacy and Reduced Side-Effects. *Acta Biomater.* **2014**, *10* (3), 1392–1402. https://doi.org/10.1016/j.actbio.2013.11.026.
(17) Shao, K.; Ding, N.; Huang, S.; Ren, S.; Zhang, Y.; Kuang, Y.; Guo, Y.; Ma, H.; An, S.; Li, Y.; Jiang, C. Smart Nanodevice Combined Tumor-Specific Vector with Cellular Microenvironment-Triggered Property for Highly Effective Antiglioma Therapy. *ACS Nano* **2014**, *8* (2), 1191–1203. https://doi.org/10.1021/nn406285x.
(18) Lv, S.; Tang, Z.; Li, M.; Lin, J.; Song, W.; Liu, H.; Huang, Y.; Zhang, Y.; Chen, X. Co-Delivery of Doxorubicin and Paclitaxel by PEG-Polypeptide Nanovehicle for the Treatment of Non-Small Cell Lung Cancer. *Biomaterials* **2014**, *35* (23), 6118–6129. https://doi.org/10.1016/j.biomaterials.2014.04.034.
(19) Bakewell, S. J.; Carie, A.; Costich, T. L.; Sethuraman, J.; Semple, J. E.; Sullivan, B.; Martinez, G. V.; Dominguez-Viqueira, W.; Sill, K. N. Imaging the Delivery of Drug-Loaded, Iron-Stabilized Micelles. *Nanomedicine: NBM* **2017**, *13* (4), 1353–1362. https://doi.org/10.1016/j.nano.2017.01.009.
(20) Jeong, Y.; Seo, S.; Park, I.; Lee, H.; Kang, I.; Akaike, T.; Cho, C. Cellular Recognition of Paclitaxel-Loaded Polymeric Nanoparticles Composed of Poly(γ-Benzyl L-Glutamate) and Poly(Ethylene Glycol) Diblock Copolymer Endcapped with Galactose Moiety. *Int. J. Pharm.* **2005**, *296* (1–2), 151–161. https://doi.org/10.1016/j.ijpharm.2005.02.027.
(21) Barz, M.; Luxenhofer, R.; Zentel, R.; Vicent, M. J. Overcoming the PEG-Addiction: Well-Defined Alternatives to PEG, from Structure–Property Relationships to Better Defined Therapeutics. *Polym. Chem.* **2011**, *2* (9), 1900–1918. https://doi.org/10.1039/C0PY00406E.
(22) Weber, B.; Birke, A.; Fischer, K.; Schmidt, M.; Barz, M. Solution Properties of Polysarcosine: From Absolute and Relative Molar Mass Determinations to Complement Activation. *Macromolecules* **2018**, *51* (7), 2653–2661. https://doi.org/10.1021/acs.macromol.8b00258.
(23) Birke, A.; Ling, J.; Barz, M. Polysarcosine-Containing Copolymers: Synthesis, Characterization, Self-Assembly, and Applications. *Prog. Polym. Sci.* **2018**, *81*, 163–208. https://doi.org/10.1016/j.progpolymsci.2018.01.002.
(24) Sill, K. N.; Sullivan, B. T. inventors; Tyndall Formulation Services, LLC assignee. Polymer Excipients for Drug Delivery Applications. U.S. Patent No. 10,836,869 B1 (filed Jan. 10, 2020).
(25) Barbosa, M. E. M.; Montembault, V.; Cammas-Marion, S.; Ponchel, G.; Fontaine, L. Synthesis and Characterization of Novel Poly(γ-Benzyl-L-Glutamate) Derivatives Tailored for the Preparation of Nanoparticles of Pharmaceutical Interest. *Polym. Int.* **2007**, *56* (3), 317–324. https://doi.org/10.1002/pi.2133.

(26) Segura-Sánchez, F.; Montembault, V.; Fontaine, L.; Martínez-Barbosa, M. E.; Bouchemal, K.; Ponchel, G. Synthesis and Characterization of Functionalized Poly(γ-Benzyl-L-Glutamate) Derivates and Corresponding Nanoparticles Preparation and Characterization. *Int. J. Pharm.* **2010**, *387* (1), 244–252. https://doi.org/10.1016/j.ijpharm.2009.12.016.

(27) Goñi-de-Cerio, F.; Mariani, V.; Cohen, D.; Madi, L.; Thevenot, J.; Oliveira, H.; Uboldi, C.; Giudetti, G.; Coradeghini, R.; Garanger, E.; Rossi, F.; Portugal-Cohen, M.; Oron, M.; Korenstein, R.; Lecommandoux, S.; Ponti, J.; Suárez-Merino, B.; Heredia, P. Biocompatibility Study of Two Diblock Copolymeric Nanoparticles for Biomedical Applications by in Vitro Toxicity Testing. *J. Nanoparticle Res.* **2013**, *15* (11), 1–17. https://doi.org/10.1007/s11051-013-2036-0.

(28) Kakkar, D.; Mazzaferro, S.; Thevenot, J.; Schatz, C.; Bhatt, A.; Dwarakanath, B. S.; Singh, H.; Mishra, A. K.; Lecommandoux, S. Amphiphilic PEO-b-PBLG Diblock and PBLG-b-PEO-b-PBLG Triblock Copolymer Based Nanoparticles: Doxorubicin Loading and In Vitro Evaluation. *Macromol. Biosci.* **2015**, *15* (1), 124–137. https://doi.org/10.1002/mabi.201400451.

(29) Sill, K. N.; Sullivan, B.; Carie, A.; Semple, J. E. Synthesis and Characterization of Micelle-Forming PEG-Poly(Amino Acid) Copolymers with Iron-Hydroxamate Cross-Linkable Blocks for Encapsulation and Release of Hydrophobic Drugs. *Biomacromolecules* **2017**, *18* (6), 1874–1884. https://doi.org/10.1021/acs.biomac.7b00317.

(30) Fenaroli, F.; Repnik, U.; Xu, Y.; Johann, K.; Herck, S. V.; Dey, P.; Skjeldal, F. M.; Frei, D. M.; Bagherifam, S.; Kocere, A.; Haag, R.; Geest, B. G. D.; Barz, M.; Russell, D. G.; Griffiths, G. Enhanced Permeability and Retention-like Extravasation of Nanoparticles from the Vasculature into Tuberculosis Granulomas in Zebrafish and Mouse Models. *ACS Nano* **2018**, *12* (8), 8646–8661. https://doi.org/10.1021/acsnano.8b04433.

(31) Dal, N.-J. K.; Speth, M.; Johann, K.; Barz, M.; Beauvineau, C.; Wohlmann, J.; Fenaroli, F.; Gicquel, B.; Griffiths, G.; Alonso-Rodriguez, N. The Zebrafish Embryo as an in Vivo Model for Screening Nanoparticle-Formulated Lipophilic Anti-Tuberculosis Compounds. *Disease Models & Mechanisms* **2022**, *15* (1), dmm049147. https://doi.org/10.1242/dmm.049147.

(32) Johann, K.; Bohn, T.; Shahneh, F.; Luther, N.; Birke, A.; Jaurich, H.; Helm, M.; Klein, M.; Raker, V. K.; Bopp, T.; Barz, M.; Becker, C. Therapeutic Melanoma Inhibition by Local Micelle-Mediated Cyclic Nucleotide Repression. *Nat. Commun.* **2021**, *12* (1), 5981. https://doi.org/10.1038/s41467-021-26269-w.

(33) Gref, R.; Lück, M.; Quellec, P.; Marchand, M.; Dellacherie, E.; Harnisch, S.; Blunk, T.; Müller, R. H. 'Stealth' Corona-Core Nanoparticles Surface Modified by Polyethylene Glycol (PEG): Influences of the Corona (PEG Chain Length and Surface Density) and of the Core Composition on Phagocytic Uptake and Plasma Protein Adsorption. *Colloids Surf. B Biointerfaces* **2000**, *18* (3), 301–313. https://doi.org/10.1016/S0927-7765(99)00156-3.

(34) Bertrand, N.; Grenier, P.; Mahmoudi, M.; Lima, E. M.; Appel, E. A.; Dormont, F.; Lim, J.-M.; Karnik, R.; Langer, R.; Farokhzad, O. C. Mechanistic Understanding of in Vivo Protein Corona Formation on Polymeric Nanoparticles and Impact on Pharmacokinetics. *Nat. Commun.* **2017**, *8* (1), 777. https://doi.org/10.1038/s41467-017-00600-w.

(35) Klemm, P.; Behnke, M.; Solomun, J. I.; Bonduelle, C.; Lecommandoux, S.; Traeger, A.; Schubert, S. Self-Assembled PEGylated Amphiphilic Polypeptides for Gene Transfection. *J. Mater. Chem. B* **2021**, *9* (39), 8224–8236. https://doi.org/10.1039/D1TB01495A.

(36) Habraken, G. J. M.; Wilsens, K. H. R. M.; Koning, C. E.; Heise, A. Optimization of N-Carboxyanhydride (NCA) Polymerization by Variation of Reaction Temperature and Pressure. *Polym. Chem.* **2011**, *2* (6), 1322–1330. https://doi.org/10.1039/C1PY00079A.

(37) Habraken, G. J. M.; Peeters, M.; Dietz, C. H. J. T.; Koning, C. E.; Heise, A. How Controlled and Versatile Is N-Carboxy Anhydride (NCA) Polymerization at 0 °C? Effect of Temperature on Homo-, Block- and Graft (Co)Polymerization. *Polym. Chem.* **2010**, *1* (4), 514–524. https://doi.org/10.1039/B9PY00337A.

(38) Le Fer, G.; Portes, D.; Goudounet, G.; Guigner, J.-M.; Garanger, E.; Lecommandoux, S. Design and Self-Assembly of PBLG-b-ELP Hybrid Diblock Copolymers Based on Synthetic and Elastin-like Polypeptides. *Org. Biomol. Chem.* **2017**, *15* (47), 10095–10104. https://doi.org/10.1039/C7OB01945A.

(39) Vayaboury, W.; Giani, O.; Cottet, H.; Deratani, A.; Schué, F. Living Polymerization of α-Amino Acid N-Carboxyanhydrides (NCA) upon Decreasing the Reaction Temperature. *Macromol. Rapid Commun.* **2004**, *25* (13), 1221–1224. https://doi.org/10.1002/marc.200400111.

(40) Peyret, A.; Trant, J. F.; Bonduelle, C. V.; Ferji, K.; Jain, N.; Lecommandoux, S.; Gillies, E. R. Synthetic Glycopolypeptides: Synthesis and Self-Assembly of Poly(γ-Benzyl-L-Glutamate)-Glycosylated Dendron Hybrids. *Polym. Chem.* **2015**, *6* (45), 7902–7912. https://doi.org/10.1039/C5PY01060H.

(41) Huesmann, D.; Birke, A.; Klinker, K.; Türk, S.; Räder, H. J.; Barz, M. Revisiting Secondary Structures in NCA Polymerization: Influences on the Analysis of Protected Polylysines. *Macromolecules* **2014**, *47* (3), 928–936. https://doi.org/10.1021/ma5000392.
(42) Bauer, T. A.; Imschweiler, J.; Muhl, C.; Weber, B.; Barz, M. Secondary Structure-Driven Self-Assembly of Thiol-Reactive Polypept(o)Ides. *Biomacromolecules* **2021**, *22* (5), 2171–2180. https://doi.org/10.1021/acs.biomac.1c00253.
(43) Miyazawa, T.; Blout, E. R. The Infrared Spectra of Polypeptides in Various Conformations: Amide I and II Bands. *J. Am. Chem. Soc.* **1961**, *83* (3), 712–719. https://doi.org/10.1021/ja01464a042.
(44) Bonduelle, C. Secondary Structures of Synthetic Polypeptide Polymers. *Polym. Chem.* **2018**, *9* (13), 1517–1529. https://doi.org/10.1039/C7PY01725A.
(45) Gaucher, G.; Dufresne, M.-H.; Sant, V. P.; Kang, N.; Maysinger, D.; Leroux, J.-C. Block Copolymer Micelles: Preparation, Characterization and Application in Drug Delivery. *J. Control. Release* **2005**, *109* (1–3), 169–188. https://doi.org/10.1016/j.jconrel.2005.09.034.
(46) Mai, Y.; Eisenberg, A. Self-Assembly of Block Copolymers. *Chem. Soc. Rev.* **2012**, *41* (18), 5969–5985. https://doi.org/10.1039/C2CS35115C.
(47) Hwang, D.; Ramsey, J. D.; Kabanov, A. V. Polymeric Micelles for the Delivery of Poorly Soluble Drugs: From Nanoformulation to Clinical Approval. *Adv. Drug Deliv. Rev.* **2020**, *156*, 80–118. https://doi.org/10.1016/j.addr.2020.09.009.
(48) Huesmann, D.; Sevenich, A.; Weber, B.; Barz, M. A Head-to-Head Comparison of Poly(Sarcosine) and Poly(Ethylene Glycol) in Peptidic, Amphiphilic Block Copolymers. *Polymer* **2015**, *67*, 240–248. https://doi.org/10.1016/j.polymer.2015.04.070.
(49) Weber, B.; Kappel, C.; Scherer, M.; Helm, M.; Bros, M.; Grabbe, S.; Barz, M. PeptoSomes for Vaccination: Combining Antigen and Adjuvant in Polypept(o)Ide-Based Polymersomes. *Macromol. Biosci.* **2017**, *17* (10), 1700061. https://doi.org/10.1002/mabi.201700061.
(50) Cauchois, O.; Segura-Sanchez, F.; Ponchel, G. Molecular Weight Controls the Elongation of Oblate-Shaped Degradable Poly(γ-Benzyl-L-Glutamate) Nanoparticles. *Int. J. Pharm.* **2013**, *452* (1), 292–299. https://doi.org/10.1016/j.ijpharm.2013.04.074.
(51) Schäfer, O.; Klinker, K.; Braun, L.; Huesmann, D.; Schultze, J.; Koynov, K.; Barz, M. Combining Orthogonal Reactive Groups in Block Copolymers for Functional Nanoparticle Synthesis in a Single Step. *ACS Macro Lett.* **2017**, *6* (10), 1140–1145. https://doi.org/10.1021/acsmacrolett.7b00678.
(52) Konno, T.; Watanabe, J.; Ishihara, K. Enhanced Solubility of Paclitaxel Using Water-Soluble and Biocompatible 2-Methacryloyloxyethyl Phosphorylcholine Polymers. *J. Biomed. Mater. Res. A* **2003**, *65* (2), 209–214. https://doi.org/10.1002/jbm.a.10481.
(53) European Medicines Agency. *ICH Q3C (R6) Residual solvents*. https://www.ema.europa.eu/en/ich-q3c-r6-residual-solvents (accessed 2021-09-08).

CRediT author statement

Coralie Lebleu: Conceptualization of the study, methodology of preparation and characterization of nanoparticles, investigation and validation preparation and characterization of nanoparticles, Supervision, Writing – Original Draft, Writing - Review & Editing
Laetitia Plet: Methodology of polymerization, investigation and validation of preparation and characterization of polymers, Writing – Original Draft, Writing - Review & Editing
Florène Moussy: Investigation and validation of preparation and characterization of nanoparticles
Gaëtan Gitton: Investigation and validation of preparation and characterization of polymers
Rudy da Costa Moreira: Methodology and validation of UPLC and SEC experiments
Ludmilla Guduff: Methodology and validation of NMR DOSY
Barbara Burlot: Investigation and validation of SEC of polymers and HS-GC of nanoparticles
Rodolphe Godiveau: Investigation and validation of preparation and characterization of polymers
Aïnhoa Merry: Investigation and validation of preparation and characterization of nanoparticles
Sébastien Lecommandoux: Supervision, Writing - Review & Editing
Gauthier Errasti: Conceptualization of the study, Supervision, Writing - Review & Editing, Project administration
Christiane Philippe: Methodology of polymerization, Supervision, Project administration
Thomas Delacroix: Conceptualization of the study, Supervision, Writing - Review & Editing, Project administration
Raj Chakrabarti: Conceptualization of the study, Supervision, Writing - Review & Editing, Project administration

No conflicts to report